

Structures of metabotropic GABA_B receptor

Makaía M. Papasergi-Scott^{1,2,4}, Michael J. Robertson^{1,2,4}, Alpay B. Seven^{1,2}, Ouliana Panova^{1,2}, Jesper M. Mathiesen³, Georgios Skiniotis^{1,2*}

¹ Department of Molecular and Cellular Physiology, Stanford University School of Medicine, Stanford, CA 94305, USA.

² Department of Structural Biology, Stanford University School of Medicine, Stanford, CA 94305, USA.

³ Department of Drug Design and Pharmacology, Faculty of Health and Medical Sciences, University of Copenhagen, Copenhagen, Denmark.

⁴ These authors contributed equally to this work.

* To whom correspondence should be addressed: yiorgo@stanford.edu

Abstract

GABA (γ -aminobutyric acid) stimulation of the metabotropic GABA_B receptor results in prolonged inhibition of neurotransmission that is central to brain physiology. GABA_B belongs to the Family C of G protein-coupled receptors (GPCRs), which operate as dimers to relay synaptic neurotransmitter signals into a cellular response through the binding and activation of heterotrimeric G proteins. GABA_B, however, is unique in its function as an obligate heterodimer in which agonist binding and G protein activation take place on distinct subunits. Here we show structures of heterodimeric and homodimeric full-length GABA_B receptors. Complemented by cellular signaling assays and atomistic simulations, the structures reveal an essential role for the GABA_B extracellular loop 2 (ECL2) in relaying structural transitions by ordering the linker connecting the extracellular ligand-binding domain to the transmembrane region. Furthermore, the ECL2 of both GABA_B subunits caps and interacts with the hydrophilic head of a phospholipid occupying the extracellular half of the transmembrane domain, thereby providing a potentially crucial link between ligand binding and the receptor core that engages G protein. These results provide a starting framework to decipher mechanistic modes of signal transduction mediated by GABA_B dimers and have important implications for rational drug design targeting these receptors.

Introduction

Normal brain function depends on the proper balance and integration of excitatory and inhibitory neurotransmission¹, a form of intracellular signaling mediated by the action of neurotransmitters on ion channels and GPCRs. The neurotransmitter γ -aminobutyric acid (GABA) is primarily responsible for synaptic inhibition throughout the nervous system via its actions on GABA_A ion channels and pre- and postsynaptic GABA_B receptors. Upon GABA stimulation, GABA_B receptors initiate intracellular signaling via the G_{i/o} class of heterotrimeric G proteins^{2,3}, which act through the inhibition of adenylyl cyclase and voltage-gated Ca²⁺ channels, as well as the opening of G protein-coupled inward rectifying potassium channels⁴. Altogether, GABA_B signaling produces a prolonged decrease in neuronal excitability and modulates the release of neurotransmitters in the central nervous system. Abnormal execution of GABA_B signaling causes multiple neuropsychiatric diseases⁵, and the receptor is an attractive drug target for a range of disorders including drug addiction, pain, epilepsy, spasticity, anxiety, and gastroesophageal reflux disease⁶⁻⁸. In particular, the GABA_B agonist baclofen has been employed as an effective clinical therapeutic for the treatment of muscle spasticity^{8,9}.

The Family C of GPCRs represents a small group of ~20 receptors that engage small molecule agonists, and includes GABA_B, the metabotropic glutamate receptors (mGlu1-8), the calcium sensing receptor (CaSR), as well as two taste and several orphan receptors^{10,11}. Family C receptors are unusual in that they operate as obligate dimers, with each subunit composed of a bi-lobed extracellular ligand-binding domain termed the Venus flytrap (VFT) and the common 7-transmembrane domain (7TM) of GPCRs connected via a linker region¹². Crystallographic studies of VFTs from various Family C members, including GABA_B, show that agonist binding rearranges the VFTs in a way that would bring the linker regions into close proximity^{13,14}. All Family C GPCRs contain a cysteine-rich domain (CRD) within the linker region, with the exception of GABA_B which only has a relatively short linker. Our recent cryoEM structures of mGlu5 showed that the CRD interacts with extracellular loop 2 (ECL2) of the transmembrane region, thereby providing the rigidity required for transducing conformational changes 120 Å from the

ligand-binding site on the VFT to the 7TM domain where G protein activation occurs¹⁵. Given that GABA_B lacks a CRD, the structural communication between an agonist-bound VFT and the 7TM domains remains unclear.

Furthermore, unlike other Family C GPCRs, GABA_B is an obligate heterodimer comprised of two dissimilar subunits, GABA_{B1} and GABA_{B2}, that must associate via intracellular C-terminal coil-coil domains in order to localize to the plasma membrane¹⁶. GABA_B is unique in that agonist binding occurs only on the VFT of GABA_{B1}, while G protein coupling and activation occurs exclusively through GABA_{B2}^{17,18}. Thus, besides its pharmacological interest, GABA_B presents an ideal model system to study trans-activation mechanisms in the context of dimeric Family C GPCRs. These studies, however, are limited by the lack of structural information on full-length GABA_B, restricting our ability to understand how agonist binding to GABA_{B1} results in G protein activation on the intracellular side of GABA_{B2}. In the present study we employed single-particle cryo-electron microscopy (cryoEM), atomistic simulations, and cellular signaling assays to obtain structural and mechanistic insights into full-length GABA_B receptor complexes.

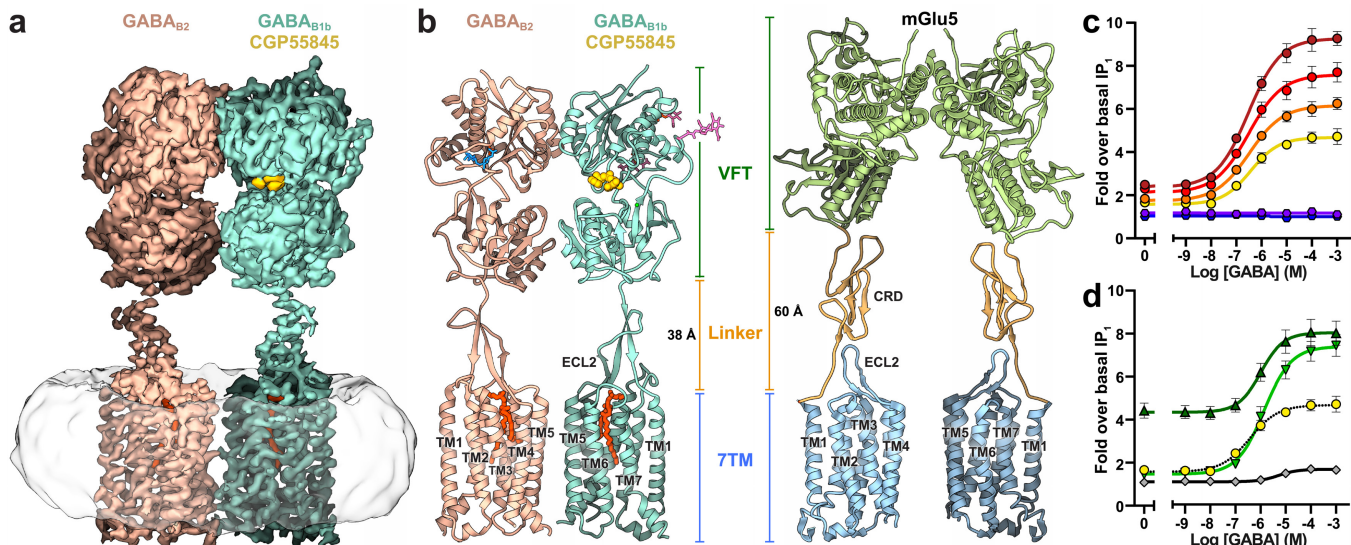
Results and Discussion

The ligand-binding subunit GABA_{B1} has two isoforms, GABA_{B1a} and GABA_{B1b}, differing only in the presence of two short consensus repeats at the N-terminus that localize the GABA_{B1a} isoform to the presynapse¹⁹. For structural studies, we designed recombinant constructs of human GABA_{B1b} and GABA_{B2} with a C-terminal hexa-histidine tag on GABA_{B1b} and an N-terminal Flag epitope (DYKDDDD) tag on GABA_{B2}. The constructs were co-expressed in *Spodoptera frugiperda* (Sf9) insect cells, and the GABA_B heterodimer was purified by tandem affinity-chromatography in the presence of the inverse agonist CGP55845²⁰ to aid receptor stability.

The structure of the inactive GABA_B heterodimer solubilized in glyco-diosgenin (GDN) detergent was determined by cryoEM at a global indicated resolution of 3.6 Å (Fig. 1, Supplemental Figs. 1 and 2a, Supplemental Table 1). The cryoEM map resolved the entire GABA_B apart from the C-terminal coil-coil

domain that appears to have a flexible disposition in relation to the transmembrane regions. Additionally, we obtained a focused map of the extracellular region at a resolution of 3.5 Å, which provided improved density for the linker regions and assisted with modeling (Supplemental Fig. 1). The asymmetric protomers, GABA_{B1} and GABA_{B2}, share a similar secondary structure and arrangement but are distinguished by differential glycosylation and the presence of a well-resolved density within the ligand-binding pocket of the GABA_{B1} VFT domain that is absent in GABA_{B2} (Fig. 1, Supplemental Fig. 3, Supplemental Fig. 4a). The upper VFT lobes of GABA_B form a junction, while the lower VFT lobes are separated by ~20 Å (Fig. 1). To model CGP55845 into the binding pocket, we utilized GemSpot²¹, our recently developed pipeline for optimal ligand docking into electron density maps. The ligand adopts a horseshoe-like conformation, closely resembling that observed in the crystal structure of the VFT domain in complex with the inhibitor CGP54626 (PDB:4MR7)^{13,20}, which differs from CGP55845 only in a substitution of an aromatic ring in place of cyclohexane. The entire ligand is confined by W65 and W278 of GABA_{B1} that form hydrophobic interactions with the chlorinated ring of CGP55845 (Supplemental Fig. 3a, b). In addition, charged phosphate and amine moieties of CGP55845 are stabilized by a pair of hydrophilic residues deep within the VFT clamshell. Curiously, we observe a small spherical density in GABA_{B1} that appears to be interacting with the backbone carbonyl of W65 in addition to several anionic groups and a tyrosine, raising the possibility of a bound divalent cation in that location (Supplemental Fig. 3c). The presence of a metal ion would be consistent with the observation that calcium and other divalent ions affect ligand affinity^{22,23}, and examination of the deposited scattering factors for the high-resolution VFT crystal structure (PDB:4MR7) reveals positive difference density also consistent with a cation at this site¹³.

Inactive GABA_B assumes a similar overall morphology to the apo-state structure of mGlu5¹⁵, while the most substantial differences arise within the linker region (Fig. 1b). Bridging the VFT and 7TM domains, an ~20 residue linker forms a β-sheet in conjunction with the extracellular loop 2 (ECL2). Notably, the length of the GABA_B receptor ECL2 is nearly twice that of mGlu5 (Fig. 1, Supplemental Fig. 4b). The GABA_B cryoEM structure reveals that in the absence of CRDs, the β-sheet structure of the



GABA_B linker in complex with ECL2 confers the structural rigidity necessary for signal transduction. Molecular dynamics simulations support the rigidity of the β -sheet formation, as after 200 ns in all simulations the linker and ECL2 continued to adopt a stable structure even in the absence of VFT domains (Supplemental Fig. 5). To further examine the involvement of the ECL2 β -sheet structure in receptor activation, we employed a functional assay with a chimeric G_{o/q}, whereby the G_{i/o}-coupled GABA_B receptor can couple to the PLC pathway and induce IP₃ formation^{3,24}. Accumulation of the downstream metabolite IP₁ by LiCl was measured by an established assay²⁵, thereby monitoring GABA-stimulated and basal receptor activity (Fig. 1c). The expression of GABA_B subunits with ECL2 deletion was generally inhibitory to the proper trafficking of the receptor to the cell surface and we thus normalized the amount of transfected DNA to obtain similar expression levels between constructs (Supplemental Fig. 6a). The deletion of the GABA_{B1} ECL2 loop (Δ 627-634) produced an increase in basal activity but

did not affect GABA efficacy when expressed with wild-type GABA_{B2} (Fig. 1d). These findings indicate that abrogating the ECL2-linker allows flexibility in the GABA_{B1} VFT relative to the rest of the receptor dimer, resulting in activation through the GABA_{B2} VFT/7TM route in the absence of agonist²⁶. In contrast, the deletion of only the GABA_{B2} ECL2 (Δ631-638) did not affect the basal receptor activity but produced an increase in GABA efficacy and a decrease in GABA potency when compared to wild-type receptor expressed to similar levels at the cell surface, indicating that the structural rigidity of the GABA_{B2} linker region may have a partial inhibitory role (Fig. 1d, Supplemental Fig. 6a). When both receptors contain a truncated ECL2, we observed a decrease in GABA efficacy, suggesting that at least one VFT domain must be structurally coupled through the extended ECL2/linker for full activation (Fig. 1d). Collectively, these data support a bimodal transactivation mechanism of GABA_B in which agonist binding on the GABA_{B1} receptor can proceed from the GABA_{B1} VFT down to the GABA_{B1} 7TM region to enact changes in GABA_{B2} that promote G protein activation, and also activate the GABA_{B2} 7TM directly through the GABA_{B2} VFT domain.

Besides the VFTs and the C-terminal coiled-coil, we observe that inactive GABA_B forms an additional dimer interface involving interactions between TM3 and TM5 from each monomer of the heterodimer (Fig. 1, Fig. 2). This arrangement is in contrast to the structure of inactive mGlu5 receptor where the 7TM domains are separated by 16Å at their nearest point (Figs. 1b, 2a)¹⁵. The inactive GABA_B 7TM interface is formed by ionic interactions between residues on the intracellular side of TM3 and TM5 of each receptor with further stabilization through aromatic residues along the same helices (Fig. 2 b, c). Specifically, H572 (TM3) and E673 (TM5) on GABA_{B1} are in interacting proximity to H579 (TM3) and E677 (TM5) of GABA_{B2}. To probe the significance of these interactions, we mutated the TM3/TM5 interface, and performed IP₁ accumulation assays as outlined above (Fig. 2d, e, Supplemental Fig. 6). Notably, mutation of either H579 or E677 on GABA_{B2} or mutation of both E673 and H572 on GABA_{B1} increased the basal activity of the receptor, suggesting that the TM3/TM5 interface is inhibitory to signaling in the absence of agonist, which further supports the transactivation mechanism described above (Fig. 2, Supplemental Figs. 6b-d). When expressed at the cell surface alone, the H579/E677 double mutant of GABA_{B2} exhibited a slight

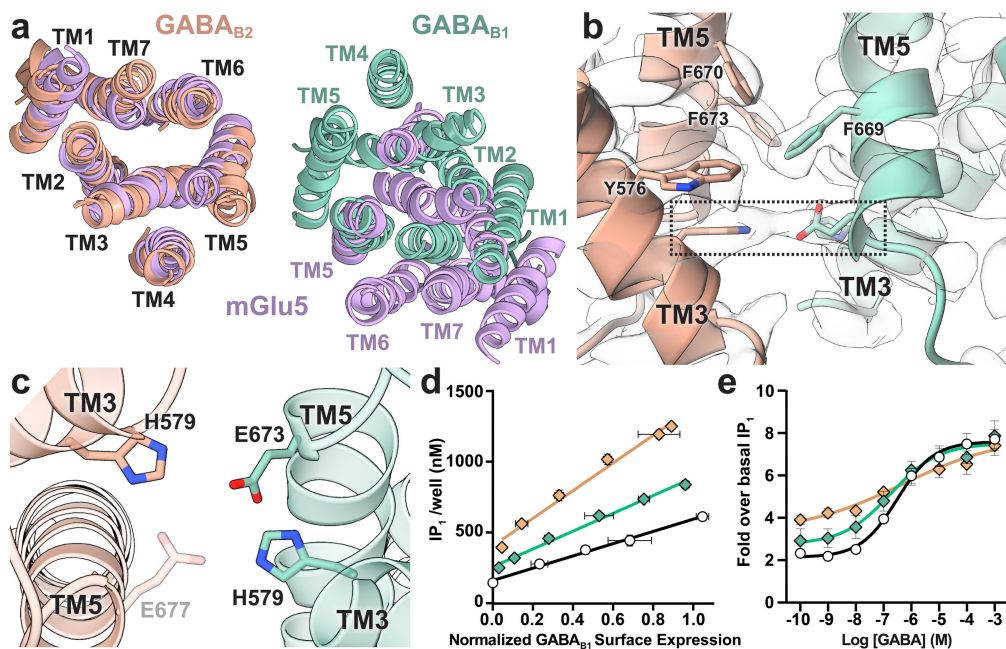


Figure 2. TM3 and TM5 stabilize an inactive-state dimer interface of GABA_B 7TM domains. **a**, Inactive-state GABA_B 7TMs (GABA_{B1}: teal, GABA_{B2}: tan) are in closer proximity compared to the 7TMs of inactive mGlu5 (purple) as shown in a top-down view. **b**, The interface between GABA_{B1} and GABA_{B2} forms a stable connection stabilized through hydrophobic interactions along TM5 helices and by polar residues on the intracellular side of TM3 and TM5 (boxed region). **c**, View of the polar interaction residues from the intracellular side of the receptor. GABA_{B2} E677 is shown for perspective; we note, however, that map density corresponding to GABA_{B2} E677 was insufficient for high-confidence modeling of its side chain. IP₁ accumulation assays illustrate differences in GABA_B TM3/5 mutants' basal activity, **d**, and GABA response, **e**. Data in **d** are representative of one experiment performed in triplicate and repeated independently at least three times with similar results. Data in **e** represent mean \pm S.E.M. from at least three independent experiments.

increase in basal activity compared to the silent GABA_{B2} (Supplemental Fig. 6d). These findings further support a role of an intra-protomer H579/E677 interaction in GABA_{B2} to assist stabilizing an auto-inhibited state of the GABA_{B2} protomer, and are in line with the lack of constitutive activity by GABA_{B2} ECL2 (Δ 631-638).

The most unexpected observation in the transmembrane region of both monomers of GABA_B is a wishbone-shaped density occupying the extracellular half of each 7TM core. The bifurcated density, which is better resolved within the GABA_{B1} helical bundle, corresponds to a phospholipid (Fig. 3, Supplemental Fig. 2). Considerations of the size and shape of the density, surrounding amino acid environment within the core of the GABA_B 7TM, and known composition of phospholipids in Sf9 insect cells, enable us to deduce with relative confidence that the bound phospholipid in GABA_{B1} and likely GABA_{B2} corresponds to phosphatidylethanolamine (PE) (Fig. 3, Supplemental Fig. 7). The observation

of PE within the transmembrane core is particularly intriguing, as no other GPCR has been shown to incorporate a two-chained phospholipid within this space. Although a lipid-activated subfamily within class A GPCRs exists, known ligands are limited to single acyl-chain lipids, eicosanoids, and sterols²⁷. Those receptors are characterized by the formation of tightly structured extracellular loops preventing ligand access from the extracellular space²⁷, as also observed in the cryoEM structure of GABA_B. Notably, residues in the extracellular loops, including ECL2, and TM3 of GABA_B coordinate the polar head group of PE resulting in a ‘lid’ over the lipid. The remaining hydrophilic atoms in the lipid appear solvent-exposed, whereas the lipid tails are buried deep into the hydrophobic portion of the transmembrane cavity (Fig. 3b, c). Additionally, a conserved TM6 tryptophan, which acts as an activating “toggle-switch” in other Family C GPCRs^{28,29}, is replaced by cysteine residues in both GABA_{B1} and GABA_{B2} receptors (Supplemental Figs. 4c, d). This replacement is essential, as any probable tryptophan rotamer at that position would clash sterically with the bound phospholipid.

The presence of lipid in the 7TM core suggests it may have a physiological role in the structural and functional integrity of the transmembrane bundles, occupying a region that corresponds to the ligand binding site in other GPCR classes (Supplemental Fig. 4). Moreover, given the crucial role of ECL2 in coordinating the linker connecting the VFT domains to the 7TM regions, it is conceivable that interactions of the phospholipid with the ECL2 have both an essential role in increasing the stability of the linker region and also participate in relaying structural transitions from the VFTs to the 7TM core. Notably, mutations designed to displace lipid tails in the 7TM core, GABA_{B1} L553W and GABA_{B2} L560W, decrease basal activity and potency of GABA while increasing GABA efficacy, whereas mutation of the arginine coordinating the head group of the phospholipids, GABA_{B1} R549A and GABA_{B2} R556A, results in increases in both GABA_B basal activity and receptor response to GABA (Fig. 3d, Supplemental Fig. 6e, f). Collectively, these results indicate that relaxation of phospholipid placement in the core affects receptor activation, and it is thus conceivable that the lipid directly modulates receptor activity as a result of ECL2 movements in native GABA_B. To further probe the role of phospholipid we employed a range of atomistic simulations with the GABA_B receptor system. We initiated simulations of the GABA_B 7TM and

linker heterodimer with the VFTs removed, both with and without lipid. The simulations without lipid typically diverged along one of two paths; the first being those simulations in which the transmembrane helices begin to collapse into the core with mean decreases in cavity volume of ~30% (Fig. 3, Supplemental Fig. 5), suggesting a strongly coupled interplay between the phospholipid and 7TM core. Alternatively, multiple simulations that started without lipid in the TMs showed lipid tails from the bilayer entering the receptor hydrophobic cavity below residue Y661, at a site akin to where the tail protrudes in our cryoEM structure. Remarkably, peripheral lipid tail insertion in simulations correlated with circumvention of the 7TM cavity collapse (Supplemental Fig. 5). In one simulation, after 200 ns we observed a lipid that had inserted both of its hydrocarbon tails into the receptor core. Extending the

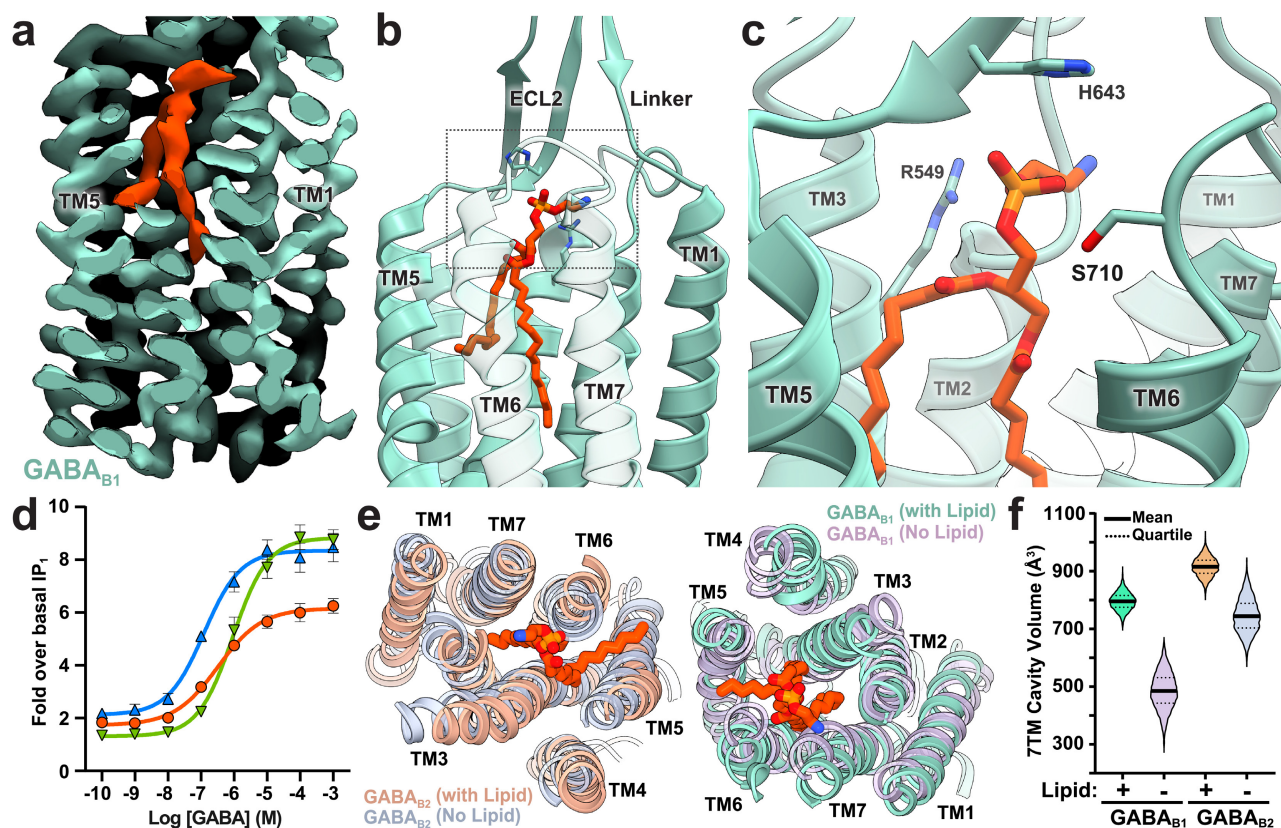


Figure 3. Phospholipid binds within the transmembrane cores of GABA_B. **a**, Side view of EM map clipped to show the location of phospholipid within GABA_{B1} of the heterodimer. Ribbon representation of PE within GABA_{B1}. **b**, with boxed region presented in panel **c** to show the structural environment of the headgroup. **d**, GABA concentration response for wild-type GABA_B (red), and mutants designed to displace phospholipid (GABA_{B1} L553W and GABA_{B2} L560W, green), or de-stabilize the phospholipid headgroup (GABA_{B1} R549A and GABA_{B2} R556A, blue). **e**, **f**, Molecular dynamics simulations show a collapse of the transmembrane cavity when lipid is absent. **e**, Representative top-down view of the GABA_B ribbon and stick model from molecular dynamics simulations at 200 ns. **f**, Violin plot of cavity volume ensemble data distribution over a 200 ns time course, for 3 simulations and 22,500 data points per condition. Data in **d** represent mean \pm S.E.M. from at least four independent experiments.

simulation by an additional 100 ns revealed the headgroup has moved over the top of the receptor, indicating lipid entry may occur as a stepwise process, with lipid tail entry sliding between TM5 and TM6 and followed by the entire lipid (Supplemental Fig. 5). Although it is probable that lipid insertion into the 7TM core occurs concurrently with helix insertion into the membrane during protein folding, these results suggest a clear tendency for phospholipids to insert at that position in a mature receptor.

Pharmaceuticals targeting the GABA_B receptor and other Family C GPCRs are proposed to function either at the orthosteric ligand binding site or allosterically within the transmembrane core, similar to class A orthosteric ligands. However, the presence of a phospholipid within the transmembrane core of GABA_B subunits would appear to occlude the binding of allosteric modulators analogous to those used to target other Family C receptors³⁰. Given this observation, future developments in targeting the GABA_B receptor will benefit from a clearer understanding of the environment of the transmembrane core, as a potential allosteric modulator would need to either displace the core lipid or bind at an alternative site.

While a pure GABA_B heterodimer was obtained by tandem affinity purification of receptor constructs with distinct tags, when using non-distinct tags to purify co-expressed GABA_{B1} and GABA_{B2} constructs we found that, in addition to the GABA_{B1/B2} heterodimer, we also purified a significant fraction (> 40%) of GABA_{B1} homodimers. In cells, an ER retention signal within the GABA_{B1} coil-coil domain prevents homodimers from reaching the plasma membrane. Thus, the presence of GABA_{B1} homodimer in our preparation is likely due to the persistence of internal membranes during the purification procedure. On the other hand, multiple studies have suggested a physiologic role for GABA_{B1} homodimers within some cell types of the nervous system and gastrointestinal tract that express GABA_{B1} isoforms in the absence of GABA_{B2}³¹⁻³⁶. Although it is yet unclear how homodimeric GABA_{B1} complex functions in the absence of GABA_{B2} G protein coupling, we sought to obtain further mechanistic insights into the GABA_B system and obtained the structure of the GABA_{B1b} homodimer at a global indicated resolution of 3.2 Å (Fig. 4, Supplemental Figs. 2 and 8, Supplemental Table 1).

The structure of the GABA_{B1} homodimer shows that both VFTs are liganded and the two receptor monomers assume a roughly 2-fold symmetric arrangement. Notably, the VFT domains adopt the same overall conformation as the crystal structure of agonist-bound GABA_B VFTs (PDB:4MS4) (Fig. 4c)¹³. Furthermore, the relative arrangement of the VFT and transmembrane regions are strikingly similar to the activated state of near full-length mGlu5¹⁵. Thus, the conformation observed in the GABA_{B1} homodimer may provide valuable hints into the architecture of the active state GABA_B receptor (Fig. 4). Compared to the heterodimer, the 7TM domains in the GABA_{B1} homodimer are rotated to form an interface between the TM6 helices of each monomer. This observation is in agreement with cross-linking experiments that identified TM6-TM6 as the 7TM interaction interface upon agonist-induced stimulation

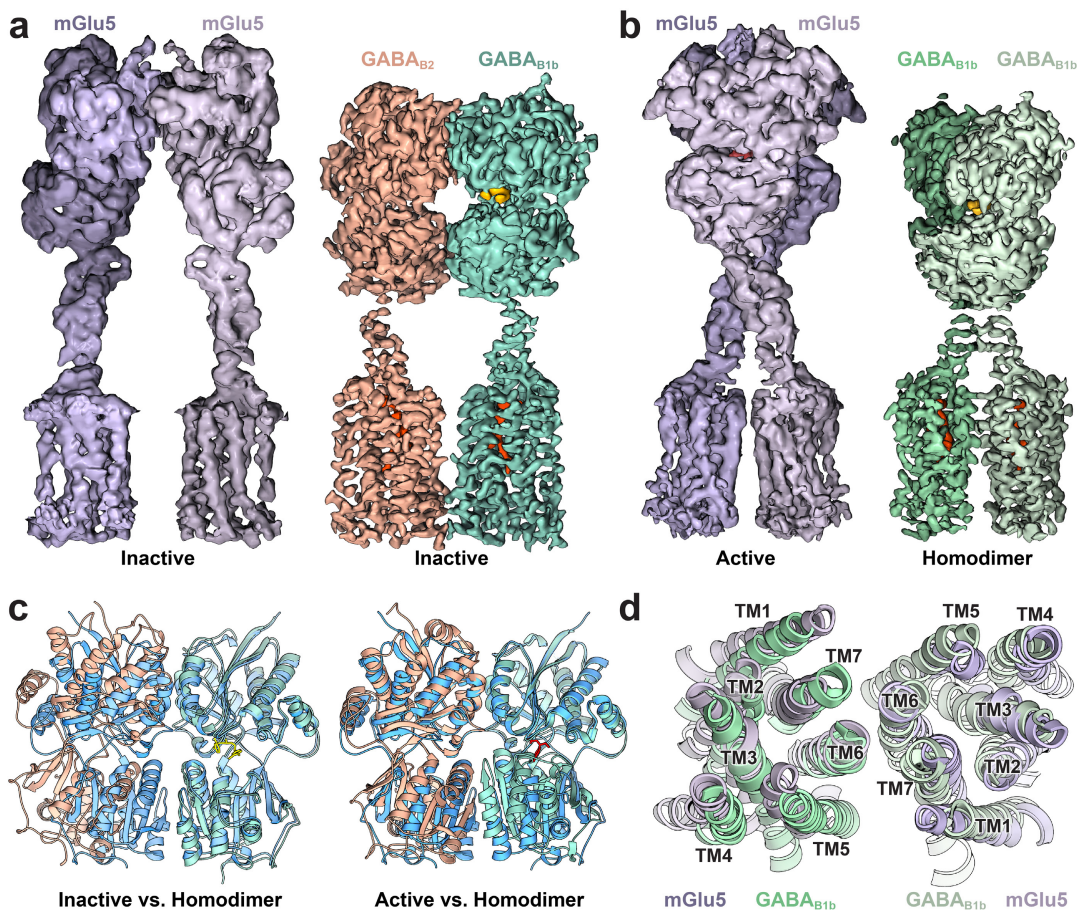


Figure 4. Inhibitor-bound GABA_{B1} homodimers adopt similar overall architecture and transmembrane interface as active mGlu5. **a**, EM maps of inactive mGlu5 (purple, EMD-0346) and GABA_B heterodimer (tan and teal); and **b**, active mGlu5 (purple, EMD-0345), and homodimeric GABA_{B1} (green). **c**, VFT overlay of crystal structures of GABA_B heterodimer (tan, teal) in inactive-state (left) and active-state (PDB:4MS4)¹³ (right) with the model of GABA_{B1} homodimer (blue). **d**, Top-down view of superposed 7TM domains of agonist-bound mGlu5 (purple) and GABA_{B1} homodimer (green).

of the heterodimer³⁷, and agrees with structural rearrangements of mGlu5 upon agonist stimulation¹⁵. Along the same lines, GABA_B chimera studies show that replacement of the GABA_{B2} VFT with that of GABA_{B1} results in increased constitutive activity of the receptor that is not additionally stimulated by GABA³⁸. Thus, the relative positioning of the VFT domains, as observed in the structure of the GABA_{B1} homodimer, appears to be sufficient to allow stabilization of an active conformation, presumably through the rigid linkage of VFT to 7TM domains to reorient the helical interface.

Collectively, our cryoEM structures, cellular signaling assays, and atomistic simulations provide crucial insights into mechanistic aspects of GABA_B signaling. The extended ECL2 and its interaction with the linker region appears to compensate for the lack of CRD in GABA_B compared to all other Family C receptors, and thus also rigidly transduce conformational changes from the VFT to the 7TM domains. The presence of phospholipid occupying the extracellular half of the 7TM core, which has not been previously observed for any GPCR, appears important for the structural integrity of the transmembrane domains in both GABA_B subunits, while also structurally coordinating the critical ECL2 region. Our findings support a model in which agonist binding to GABA_{B1} results in VFT dimer compaction that reorients the rigidly structured linker/ECL2. Such conformational change would drive the 7TM domains to twist away from an auto-inhibited state mediated by the inactive TM3/TM5 interface, thereby forming a new interface mediated by the TM6 helices. Although currently unclear, the activating transitions within the GABA_{B2} 7TM are likely mediated both through the newly formed TM6/TM6 interface and propagation through its own ECL2, as supported by our functional assays. An intriguing possibility is that the phospholipid may act as a sensor of changes in VFT and ECL2 conformations that would result in activating transitions within the 7TM domain of GABA_{B2} to prime it for G protein engagement. Addressing these questions will require further structural studies of active state heterodimer alone and in complex with G protein. The present work, along with our recent studies on mGlu5, form a starting structural framework to decipher the enigmatic signal transduction mechanism of GABA_B and Family C GPCRs in the context of full-length receptors.

Materials & Methods

Cloning

The cDNA clone for human GABA_{B2} receptor (Accession: NM_005458) in pcDNA3.1⁺ was obtained from the cDNA Resource Center (www.cdna.org); and the cDNA clone for human GABA_{B1b} was purchased from Horizon Discovery (Accession: BC050532, Clone ID: 5732186). Primers were designed to include a hemagglutinin (HA) signal sequence³⁹ in the place of authentic signal sequences of each receptor, thus removing the first 29 residues of GABA_{B1} and 41 residues of GABA_{B2}. The following primers (Integrated DNA Technologies) were used to sub-clone GABA_B constructs into the pFastBacDual vector (Invitrogen) with N-terminal Flag epitope (DYKDDDD) following the HA tag and/or C-terminal hexa-histidine (His6) tags: EcoRI-HA-Flag-GABA_{B1}, 5'-GCGCGCGAATTCAAGGACGACGATGACAAGTCCCCTCCCCCATCTCCCG-3'; GABA_{B1}-His6-Sall, 5'- GCGCGCGTCGACTTAATGATGATGATGGTGCCTTATAAAGCAAATGCAC-3'; GABA_{B1}-Sall 5'- GCGCGCGTCGACTTACTTATAAAGCAAATGCAC-3'; EcoRI-HA-FLAG-GABA_{B2}, 5'-GCGCGCGAATTCAAGGACGACGATGACAAGTGGCGCGGGCGCCCC-3'; GABA_{B2}-His6-Sall, 5'- GCGCGCGTCGACTTAATGATGATGATGGTGCAGGCCGAGACCATGAC-3'; GABA_{B2}-Sall, 5'- GCGCGCGTCGACTTACAGGCCGAGACCATGAC-3'. To generate GABA_B mutants PCR reactions were conducted with either PfuTurbo or Q5 polymerase using the following pairs of primers and pcDNA3.1⁺ containing either HA-FLAG-GABA_{B1b} or HA-HA-GABA_{B2}: GABA_{B1b} H572A, 5'-GGTGGTCGCCACGGTCTTC-3' and 5'-GAAGACCGTGGCGACCCACC-3'; GABA_{B1b} E673A, 5'-CTTGGCTTATGCTACCAAGAG-3' and 5'-CTCTGGTAGCATAAGCAAG-3'; GABA_{B2} H579A, 5'-CTGGAGAGTCGCTGCCATCTCAA-3' and 5'-TTGAAGATGGCAGCGACTCTCCAG-3'; GABA_{B2} E677A, 5'-CTTAGCTTGGCTACCCGCAAC-3' and 5'-GTTGCGGGTAGCCAAGCTAAG-3'; GABA_{B1} (Δ627-634), 5'-CTTGGCAAATGTCTCAATGGTC-3' and 5'-GTCTCTATTCTGCCAGC-3'; GABA_{B2} (Δ631-638), 5'-ATCTCCATCCGCCCTCTCC-3' and 5'-CATGCTGTACTTCTCCACTG-3'; GABA_{B1} R549A, 5'-CTGCCAGGCCGCCCTGGCTCCTG-3' and 5'-ACGAAAGGAACTGG-3'; GABA_{B2}

R556A, 5'- GCACCGTCGCTACCTGGATTCTC-3' and 5'- AAA GTG TTT CAA AGG-3'; GABA_{B1} L553W, 5'- CTCTGGCTCTGGGCCTGGCTTAG-3' and 5'-GCGGGCCTGGCAGACG-3'; GABA_{B2} L560W, 5'-GGACCTGGATTGGACCGTGGCTAC-3' and 5'-TGACGGTGCAAAGTG-3'.

Expression and Purification

Spodoptera frugiperda (Sf9) insect cells (Expression Systems) were co-infected at a density of ~2.0 x 10⁶ cells/mL with HA-FLAG-GABA_{B2} baculovirus and either HA-FLAG-GABA_{B1b}-His6 or HA-GABA_{B1b}-His6 baculovirus at a multiplicity of infection (M.O.I.) between 3.0 – 5.0. During expression, cells were treated with 5 µM CGP55845 (Hello Bio, Inc.). At 48 hours post-infection cells were harvested by centrifugation, washed once with phosphate-buffered saline containing protease inhibitors (leupeptin, soybean trypsin inhibitor, N-*p*-Tosyl-L-phenylalanine chloromethyl ketone, Tosyl-L-lysyl-chloromethane hydrochloride, phenylmethylsulfonyl fluoride, aprotinin, bestatin, pepstatin) and 5 µM CGP55845. Cell lysis was achieved through nitrogen cavitation in buffer containing 20 mM HEPES, pH 7.5, 150 mM NaCl, 1 mM EDTA, 10 µM CGP55845, 2 mM MgCl₂, nuclease, and protease inhibitors. The whole-cell lysate was centrifuged at 1,000 xg to remove nuclei and unbroken cells. The supernatant was centrifuged at 100,000 xg to isolate the membrane fraction. Membranes were resuspended by Dounce homogenization in buffer containing 20 mM HEPES, pH 7.5, 150 mM NaCl, 2 mM MgCl₂, 1 mM EDTA, 2 mg/mL iodoacetamide, 10 µM CGP55845, 1% n-Dodecyl β-D-maltoside (DDM), 0.2% Sodium cholate, 0.2% Cholesterol hemisuccinate (CHS), nuclease, and protease inhibitors. Solubilized membranes were clarified by centrifugation at 100,000 xg, and the supernatant was loaded onto a pre-equilibrated column of anti-DYKDDDDK G1 affinity resin (Genscript). The resin was washed with Buffer A (20 mM HEPES, pH7.5, 150 mM NaCl, 10 µM CGP55845, and protease inhibitors) with 0.1% DDM and 0.02% CHS. Protein was eluted with Buffer A containing 0.1% DDM, 0.02% CHS, and 0.2 mg/mL DYKDDDDK peptide. The eluate was then loaded onto a pre-equilibrated Nickel-NTA column. Resin was washed with Buffer A containing 0.1% DDM, 0.02% CHS; and the buffer was exchanged in six steps to Buffer A supplemented with 0.2% GDN, 0.02% CHS, followed by a two-step exchange into Buffer A containing

0.004% GDN, 0.0004% CHS. Protein was eluted from the Ni-NTA resin with Buffer A containing 0.004% GDN, 0.0004% CHS, and 500 mM Imidazole. The resulting eluate was concentrated by centrifugal filtration with a 50 kDa molecular weight cut off, and subsequently run on a Superose 6 size exclusion column (GE Healthcare). Samples were pre-screened for sample quality by negative stain transmission electron microscopy and then immediately prepared on cryoEM grids.

CryoEM Data Collection

For the GABA_{B1b}/GABA_{B2} heterodimer, 3.5 uL of sample was applied at a concentration of 3-5 mg/mL to glow-discharged holey carbon grids (Quantifoil R1.2/1.3). The grids were blotted using an FEI Vitrobot Mark IV (Thermo Fisher Scientific) at 18 °C and 100% humidity, and plunge frozen into liquid ethane. Two data sets were used to produce the final structure. For both data collections cryoEM imaging was performed on a Titan Krios (Thermo Fisher Scientific) electron microscope equipped with a K3 Summit direct electron detector (Gatan). The microscope was operated at 300 kV accelerating voltage, at a magnification of 57,050x in counting mode resulting in a magnified pixel size of 0.8521 Å. For the first data set, movies were obtained at a dose rate of 14.19 electrons/ Å²/sec with defocus ranging from -1.5 to -2.7 μm. The total exposure time was 3.985 sec over 57 frames per movie stack. For the second data set, movies were obtained at a dose rate of 21.43 electrons/ Å²/sec with defocus ranging from -1.2 to -2.5 μm. The total exposure time was 2.996 sec including 50 frames per movie stack.

CryoEM grids for the GABA_{B1b} homodimer at a concentration 5.0 mg/mL were prepared similar to the heterodimer. CryoEM imaging was performed on a Titan Krios electron microscope equipped with a post-column energy filter and a K2 Summit direct electron detector (Gatan). The microscope was operated at 300 kV accelerating voltage, at a magnification of 47,198x in counting mode resulting in a pixel size of 1.06 Å. Movies were obtained at a dose rate of 6.212 electrons/Å²/sec with defocus ranging from -0.9 to -2.5 μm. The total exposure time was 8.0 sec over 40 frames per movie stack. Automatic data acquisition was performed using SerialEM⁴⁰ for all data sets.

Image Processing and 3D Reconstruction

Dose-fractionated image stacks were subjected to beam-induced motion correction and dose-weighting using MotionCor2⁴¹. Contrast transfer function parameters for each non-dose weighted micrograph were determined by Gctf⁴² for the homodimer and data set #1 of the heterodimer, and by CtfFind-4.1⁴³ for data set #2 of the heterodimer. For all data sets; particle selection, 2D and 3D classification were performed on a binned dataset (pixel size 1.72Å and 4.24Å for the heterodimer and homodimer, respectively) using RELION (versions 3.0 and 3.1)⁴⁴. The two data sets for the heterodimer were processed individually before being combined following a Bayesian polishing step. A total of 538,957 particles from 1,324 micrographs and 2,062,083 particles from 8,991 micrographs were extracted using semi-automated particle selection for the heterodimer data set #1 and #2, respectively. Both particle sets were then separately subjected to three rounds of 2D classification and two rounds of 3D classification. Particles in both sets were subjected to Bayesian polishing individually and then combined for a total of 286,140 particles. The merged dataset was fit for Ctf parameters (per particle defocus and astigmatism, per micrograph *B*-factor) and estimated for anisotropic magnification and beam-tilt. A final 3D refinement was followed by post-processing using a mask that excluded the GDN micelle density. A focused refinement was also carried out using a mask encompassing the VFT and linker regions of GABA_B. For the GABA_{B1b} homodimer structure, a total of 2,278,113 particles were extracted from 5,602 micrographs using semi-automated particle selection. Particles were subjected to multiple rounds of 2D and 3D classification until a subset of 282,811 particles were selected for the final map. The particle set underwent multiple rounds of Ctf parameter fitting and was subjected to Bayesian polishing before 3D Refinement and post-processing of the final map. UCSF Chimera⁴⁵ was used for map/model visualization.

Model Building

The initial model for the VFT domain was taken from the inactive state VFT crystal structure PDB:4MR7¹³ and the initial structure of the transmembrane domain of GABA_{B1b} was generated as a homology model from the inactive cryoEM structure of mGlu5 (PDB:6N52) using Schrödinger's Prime homology modeling¹⁵. Both components were placed into the GABA_B cryoEM map using Chimera's 'fit-in-map' function. The linker, intracellular loops, and extracellular loops of GABA_{B1} were interactively adjusted into the EM map using Coot (version 0.8.9.1el)⁴⁶ and the resulting model of the GABA_{B1} Linker/7TM was then used to generate a homology model of GABA_{B2} using Schrodinger's Prime homology modeling, which was also placed into the map in Chimera. Iterative rounds of interactive model adjustment in Coot followed by real-space refinement in Phenix (version 1.17.1-3660)⁴⁷ employing secondary structure restraints in addition to the default restraints were performed to improve the modeling. Once confidence in the sidechain placement was reached for the ligand-binding cleft on GABA_{B1}, the GemSpot pipeline²¹ (Schrödinger) was used to model the inhibitor, CGP55845, into the map. After further improvement, 1-palmitoyl-2-oleoyl-sn-glycero-3-phosphoethanolamine (POPE) was modeled in the transmembrane pocket of GABA_{B1} and GABA_{B2} with the GemSpot pipeline. Final refinement was performed with Phenix⁴⁷.

Molecular Dynamics Simulations and Analysis

To prepare the system for molecular dynamics simulations, the low-resolution features of the map were used to manually build ICL2 into the model of the GABA_{B1}/GABA_{B2} inactive heterodimer using Coot. The system was then prepared in Maestro, version 2019-4 (Schrödinger) to build any stubbed sidechains and determine protonation states. The VFTs were removed from the heterodimer to produce a truncated construct starting at residues T461 for GABA_{B1b} and T468 for GABA_{B2}, thus containing only the linkers and the TM domains. The Orientations of Proteins in Membranes (OPM)⁴⁸ webserver was used to orient the system with respect to a membrane plane and the CHARMM-GUI⁴⁹ was employed to place the

system in either a 1-palmitoyl-2-oleoyl-sn-glycero-3-phosphocholine (POPC) and cholesterol bilayer or a 3:1 POPC:1-palmitoyl-2-oleoyl-sn-glycero-3-phosphoethanolamine (POPE) and cholesterol bilayer. Approximate dimensions for the system were 105 x 105 x 110 Å for a total of 240 lipid and 7 cholesterol molecules. This bilayer was then solvated in TIP3P water with 150 mM sodium chloride ions balanced to achieve charge neutrality. POPE was used for the lipid in the TM binding sites of GABA_{B1} and GABA_{B2}.

The PDB file for the full solvated system was prepared in VMD (version 1.9.3)⁵⁰ for simulation in NAMD (version 2.13)⁵¹. The OPLS-AA/M⁵² force field was used for the protein, while OPLS-AA⁵² was used for the lipids, cholesterol, and ions. Disulfide bonds were placed between C546 and C644 in GABA_{B1} and C553 and C648 in GABA_{B2} and both the N- and C- termini were blocked with capping groups. NAMD was used to run molecular dynamics simulations, where all phases employed periodic boundary conditions with non-bonded interactions smoothed starting at 10 Å to 12 Å, with long range interactions treated with the particle mesh Ewald method. Systems were minimized for 2000 steps and then slowly heated in the NPT ensemble with a Langevin thermostat and a Nosé-Hoover Langevin piston barostat set at 1 atm with a period of 50 fs and a decay of 25 fs. A 2 fs time-step was used with the SHAKE⁵³ and SETTLE⁵⁴ algorithms. Heating occurred from 0 K to 310 K in increments of 20 K with 0.4 ns of simulation at each increment. Harmonic restraints of 1 kcal/mol/Å² were used during heating on all non-hydrogen atoms of the protein and lipids. The system was then equilibrated with 1 kcal/mol/Å² harmonic restraints on all protein and lipid non-hydrogen atoms for 10 ns followed by another 10 ns of equilibration with 1 kcal/mol/Å² harmonic restraints on non-hydrogen backbone atoms. Finally, 1 kcal/mol/Å² harmonic restraints were applied to only C alpha atoms for 2 ns before being stepped down to 0.5 kcal/mol/Å² for 2 ns, 0.3 kcal/mol/Å² for 2 ns, and then removed. The first 30 ns of unrestrained molecular dynamics were also discarded as equilibration.

All trajectories were down sampled by 10x for analysis. Cavity volume was calculated with Epoch (1.0.5)⁵⁵ in VMD⁵⁰ on trajectories that had been aligned to either GABA_{B1} or GABA_{B2} from the starting structure. The cavity region was defined to include the binding region of the hydrophobic tails of the lipid.

TM-TM distances were calculated in VMD based on the CA position of residues: 3.33, 4.50, 5.40, 6.54, and 7.28 in the Ballesteros–Weinstein⁵⁶ numbering scheme.

Transfection and seeding of cells for signaling assays

HEK293 cells (ATCC® CRL-1573™) were transfected with expression vector DNAs encoding the two GABA_B receptor protomers and a chimeric G $\alpha_{q/05}$ subunit (five C-terminal amino acids of G α_q were exchanged with those of G α_0) to allow the G $\alpha_{i/o}$ -coupled GABA_B receptor to activate PLC and induce IP₃ and intracellular Ca²⁺ release³. Prior to transfection cells were brought into suspension by trypsinization and resuspension to 0.18 million cells/mL in growth medium (D-MEM, Gibco 10566016; supplemented with 10% Fetal Bovine Serum, Gibco 10270106; 1% Sodium Pyruvate, Gibco 11360039; 1% MEM Non Essential Amino Acids, Gibco 11140068; and 1% Penicillin-Streptomycin Solution, Gibco 15140122).

For each 1 mL of cell suspension transfected, a total of 1 μ g DNA in 25 μ L OptiMEM (Gibco 51985) was incubated for 20 min with a mixture of 57 μ L OptiMEM and 3 μ L FuGene6 (Promega E2692). After FuGene6/DNA complex formation, the mixture was added directly to the cell suspension, mixed thoroughly and cells seeded with 100 μ L cell suspension in appropriate 96-well plates. Of the 1 μ g DNA/mL cell suspension, the amount of expression vector DNA encoding the chimeric G $\alpha_{q/05}$ was 0.5 μ g/mL cell suspension in all experiments. The amount of GABA_B encoding DNA was varied between 7.8 ng and 0.25 μ g for each of the GABA_B receptor protomer DNAs depending on the assay and mutants tested. Empty vector DNA was added to give a total amount of 1 μ g DNA/mL cell suspension transfected. For characterization of basal activity of the TM3/5 protomer mutants, a typical gene dose experiment was performed. DNA corresponding to 62.5 ng DNA/mL cell suspension of each of the protomers (wild-type or mutants) were mixed and serially diluted 2-fold 5 times, typically down to 3.9 ng DNA/mL cell suspension. The transfected cell suspension was seeded at 100 μ g/mL both in clear poly-L-lysine coated 96-well plates for IP₁ accumulation assays and in white poly-L-lysine coated 96-well plates for cell surface ELISA assays.

IP₁ accumulation assays

The IP₁ assays for wild-type and mutant receptors was performed essentially as described¹⁵. Forty-eight hours after transfection, the growth medium was replaced with HBSS buffer (HBSS (Gibco 14025), 20 mM HEPES pH 7.5, 1 mM CaCl₂, 1 mM MgCl₂ and 0.1% BSA) supplemented with BSA to 0.5% and incubated at 37 °C for 3-4 hours.

For characterization of the TM3/TM5 protomer interface mutants for basal activity, the HBSS + 0.5% BSA buffer was replaced with 100 µL HBSS buffer, followed by addition of 50 µL HBSS buffer containing LiCl (150 mM) to give a final concentration of 50 mM LiCl. After incubation for 1 hour at 37°C the IP₁ accumulation was stopped by addition of 40 µL CisBio IP-One Tb HTRF Kit (CisBio, 62IPAPPEC) lysis buffer. The accumulated IP₁ levels were determined according to the manufacturer's instructions and as described¹⁵.

For the generation of GABA concentration response curves, the compounds were diluted in three times the final concentration in HBSS buffer containing 60 mM LiCl. The assay was started, first by replacing the HBSS + 0.5% BSA buffer with 100 µL HBSS buffer, followed by addition of 50 µL of the above compound dilutions to give a final LiCl concentration of 20 mM. The IP₁ accumulation assay was stopped and assayed as described above after incubation for 1 hour at 37 °C. Data were calculated as the amount of IP₁ formed per well or normalized to the basal IP₁ level and fitted by non-linear regression using GraphPad Prism. Results and description of statistical analyses used in this manuscript are found in Supplemental Table 2.

Cell surface ELISA assay

Surface expression levels of wild-type and mutant GABA_B receptors were determined using a direct enzyme-linked immunosorbent assay (ELISA) against the N-terminal GABA_{B1b} FLAG tag and the N-terminal GABA_{B2} HA-tag, as described⁵⁷. Transfected cells were seeded in white Poly-D-Lysine-coated 96-well plates. Forty-eight hours after transfection, cells were washed once with 100 µL/well DPBS + 1

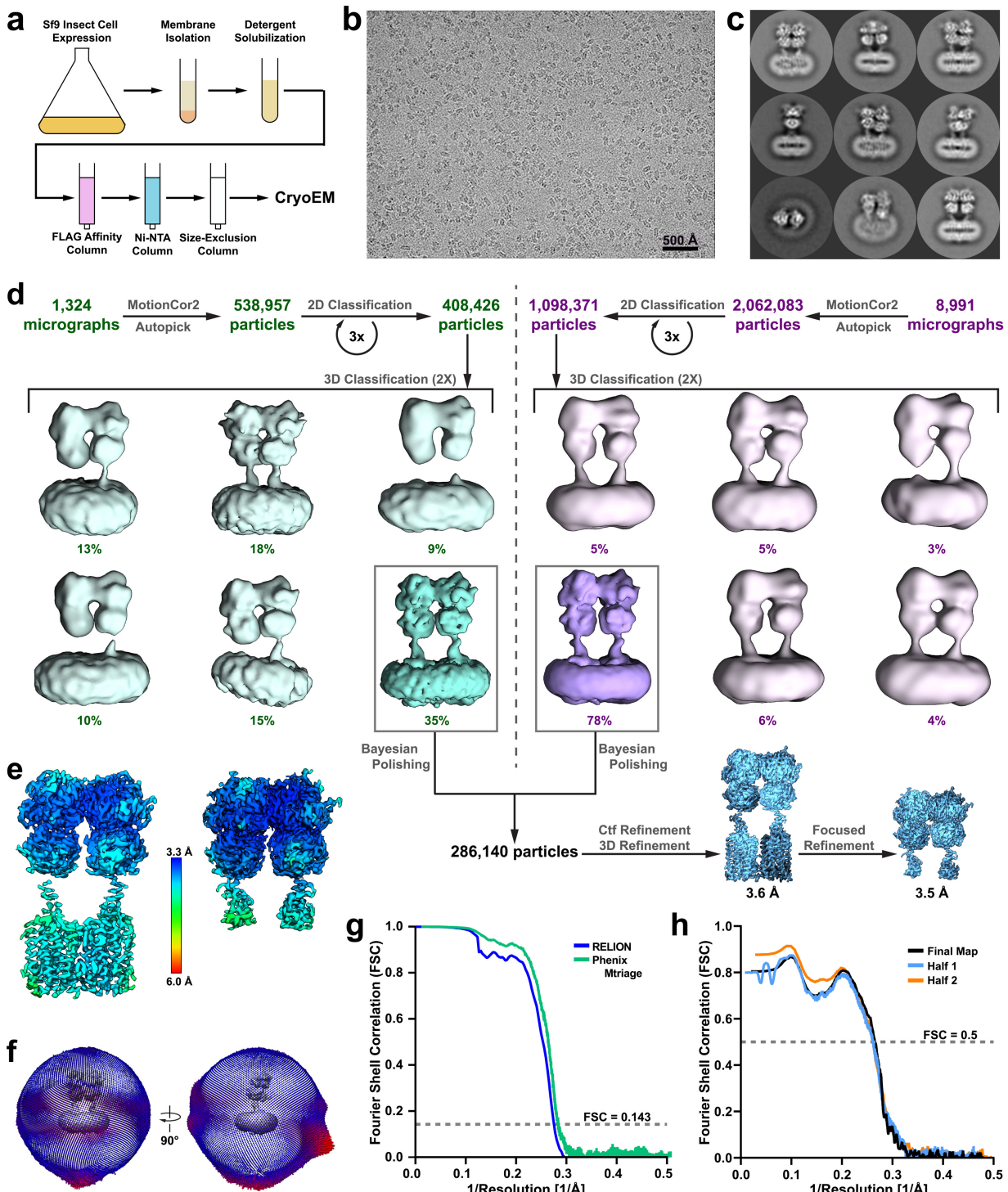
mM CaCl₂ (wash buffer). Following fixation with 50 µL/well 4% paraformaldehyde solution for 5 minutes at room temperature, cells were washed twice with 100 µL wash buffer and blocked with 100 µL/well blocking solution (3% dry-milk, 1 mM CaCl₂, 50 mM Tris-HCl, pH 7.5) for 30 minutes at room temperature, followed by addition of 75 µL/well HRP-conjugated anti-FLAG antibody (Sigma Aldrich, A8592), or HRP-conjugated anti-HA antibody (R&D systems HAM0601), both diluted 1:2000 in blocking solution, and allowed to incubate for 1 hour at room temperature. The plates were then washed four times with 100 µL/well blocking solution followed by four washes with wash buffer. The amount of surface expressed receptors was detected by adding 60 µL wash buffer and 20 µL HRP substrate (Bio-Rad, 170-5060) per well, incubating for 10 minutes and measuring of luminescence in an EnVision plate reader (Perkin Elmer).

Author contributions

M.M.P-S. designed and cloned GABA_B constructs, expressed and purified all proteins, collected and processed cryoEM data. M.J.R. built and refined the structure from cryoEM density maps and setup, performed, and analyzed molecular simulations. A.B.S. and O.P. assisted with cryoEM data collection and processing. J.M.M. performed and analyzed cellular signaling experiments. M.M.P-S., M.J.R, J.M.M., and G.S. interpreted results. M.M.P-S., M.J.R., and G.S. wrote the manuscript with J.M.M., O.P., and A.B.S. providing input. G.S. supervised the project.

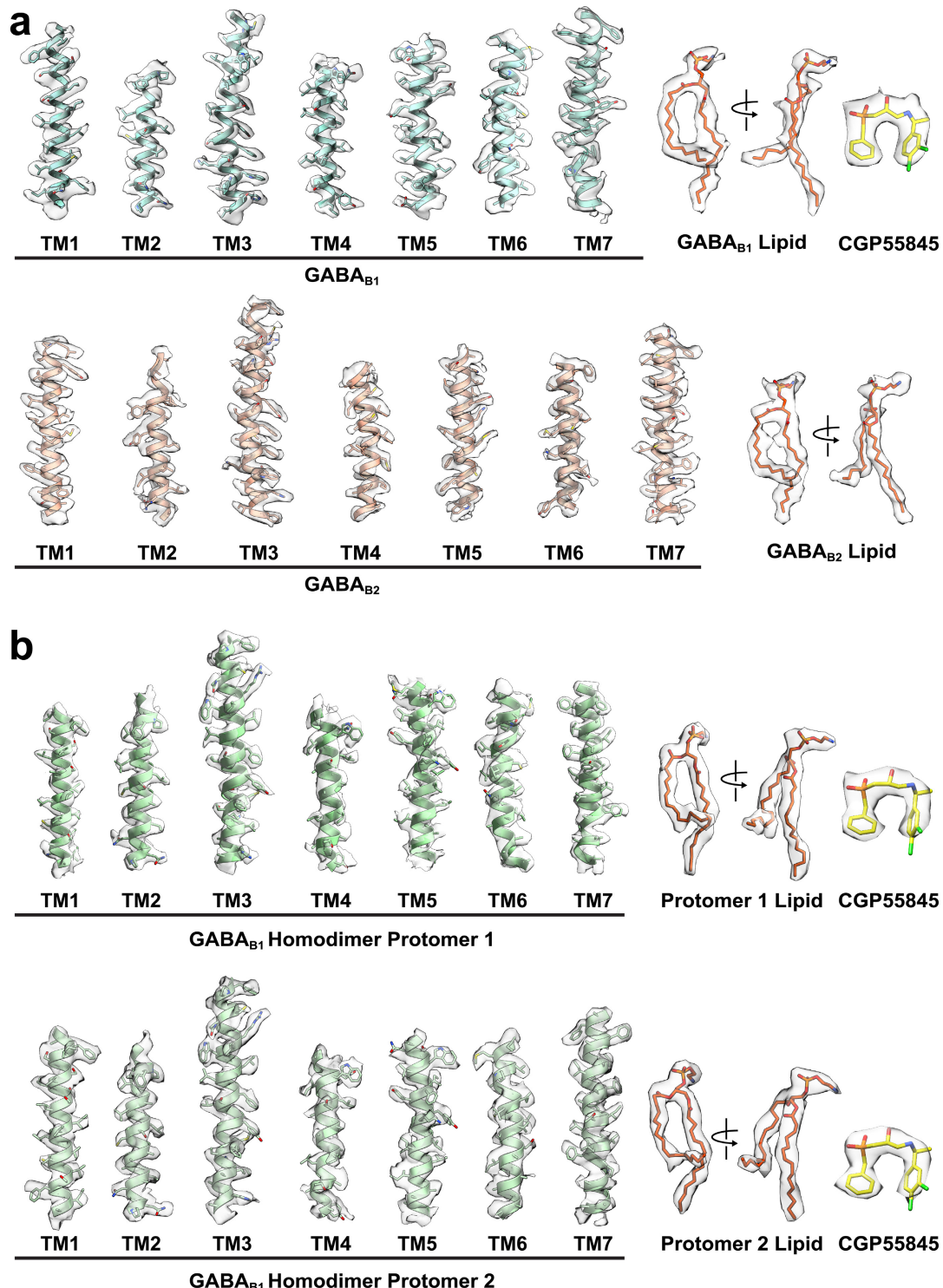
Acknowledgements

The work is supported by National Institutes of Health (NIH) grant R01 NS092695 (G.S. and J.M.M.) and used the Extreme Science and Engineering Discovery Environment (XSEDE)⁵⁸ resource comet-gpu through sdsc-comet allocation TG-MCB190153, which is supported by National Science Foundation grant number ACI-1548562. We thank Qianhui Qu for cryoEM advice and assistance.

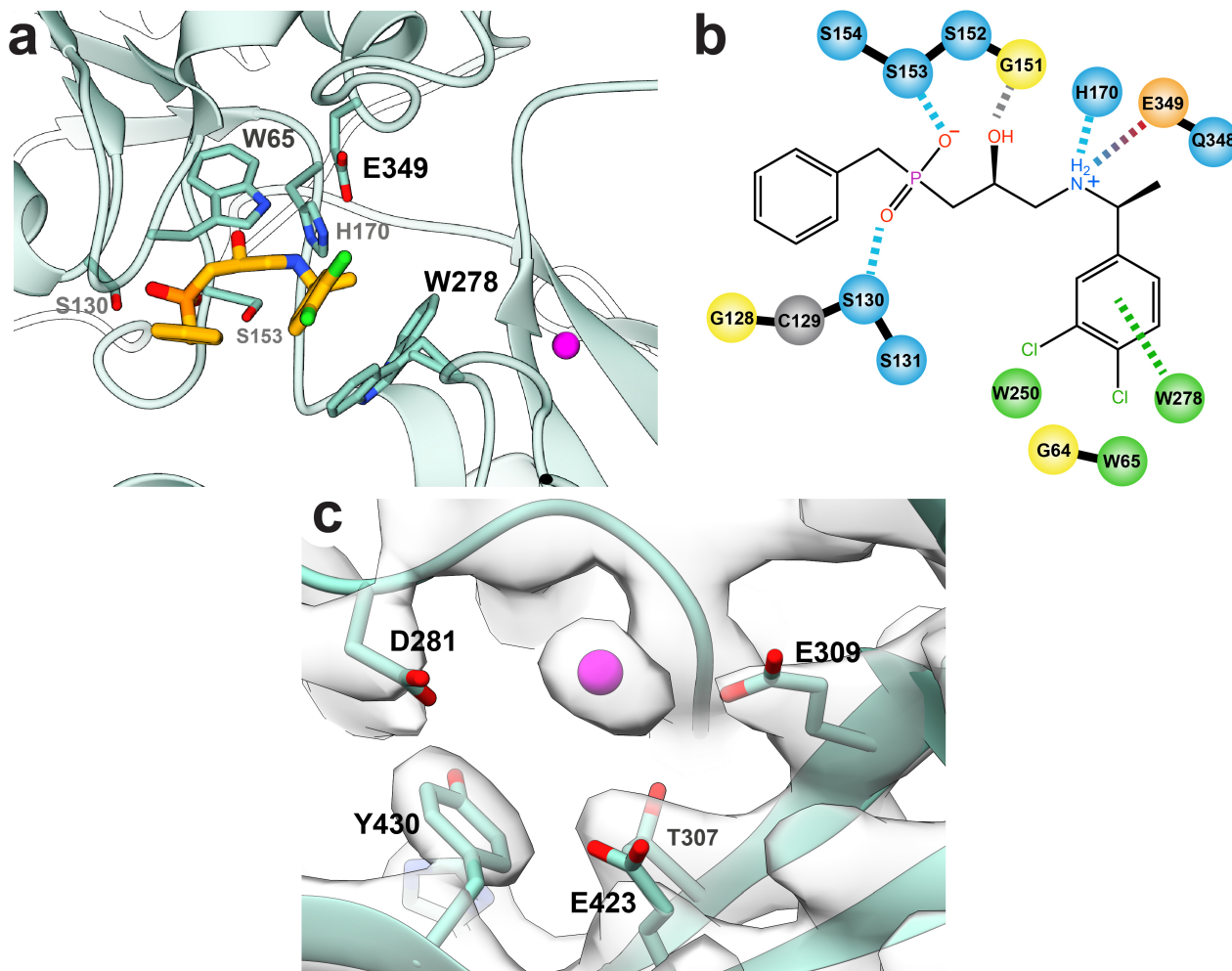


Supplemental Figure 1. Sample preparation, cryoEM processing and reconstruction of GABA_B heterodimer.

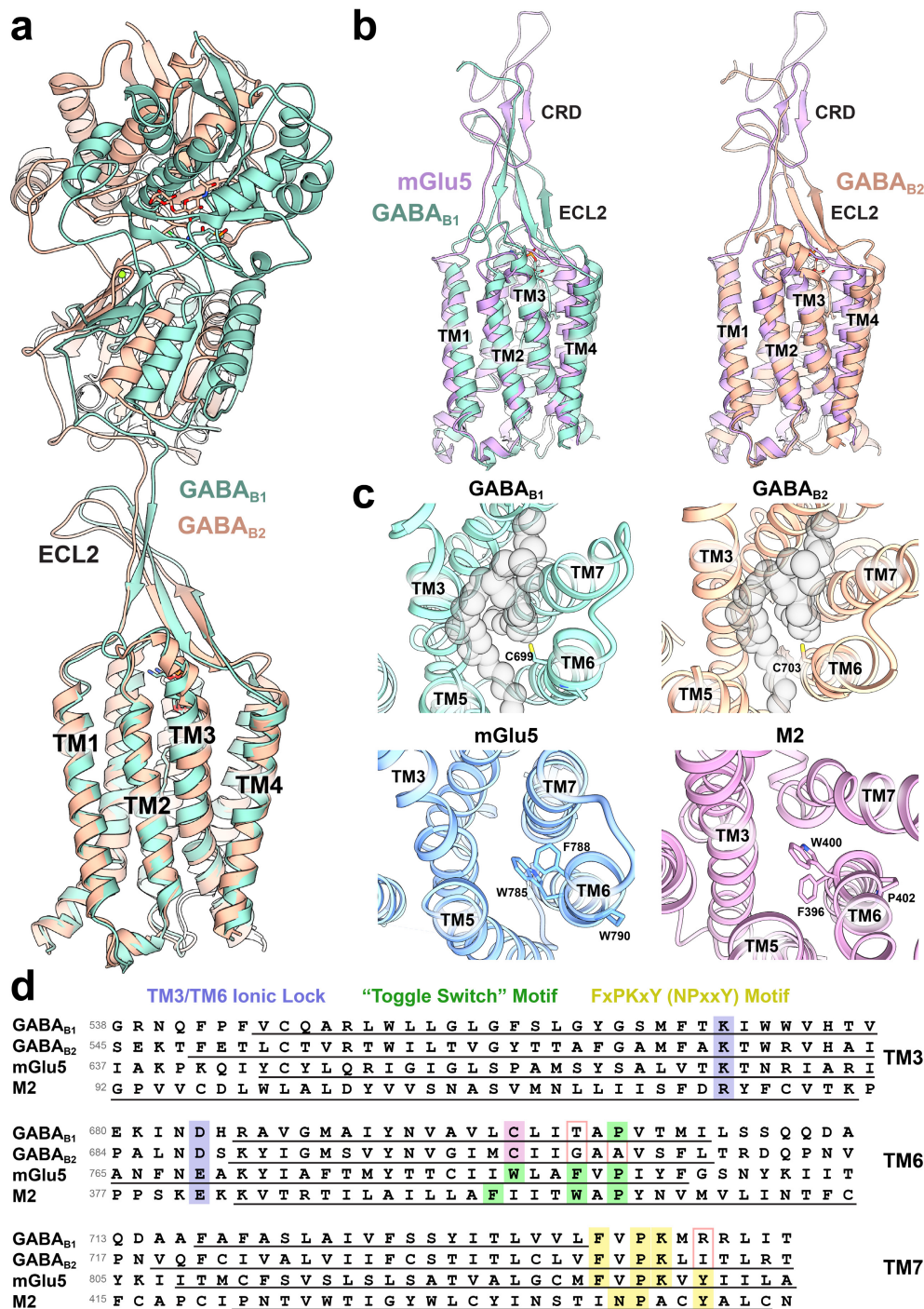
a, Purification scheme for GABA_B. Representative cryoEM micrograph (**b**) and 2D class averages (**c**) of GABA_B dimers. **d**, Flow chart outlining the cryoEM processing workflow using RELION⁵⁹, the global resolutions of the full-length structure and VFT focused structures were 3.6 Å and 3.5 Å, respectively, at 0.143 Fourier shell correlation (FSC) as calculated by RELION. **e**, Local resolution of cryoEM maps. **f**, Angular distribution of projections used in final cryoEM reconstruction. **g**, **h**, Gold standard FSC curve of half-maps calculated using RELION and Phenix Mtriage⁶⁰ (**g**), and map-to-model validation curves generated through Phenix Mtriage (**h**).



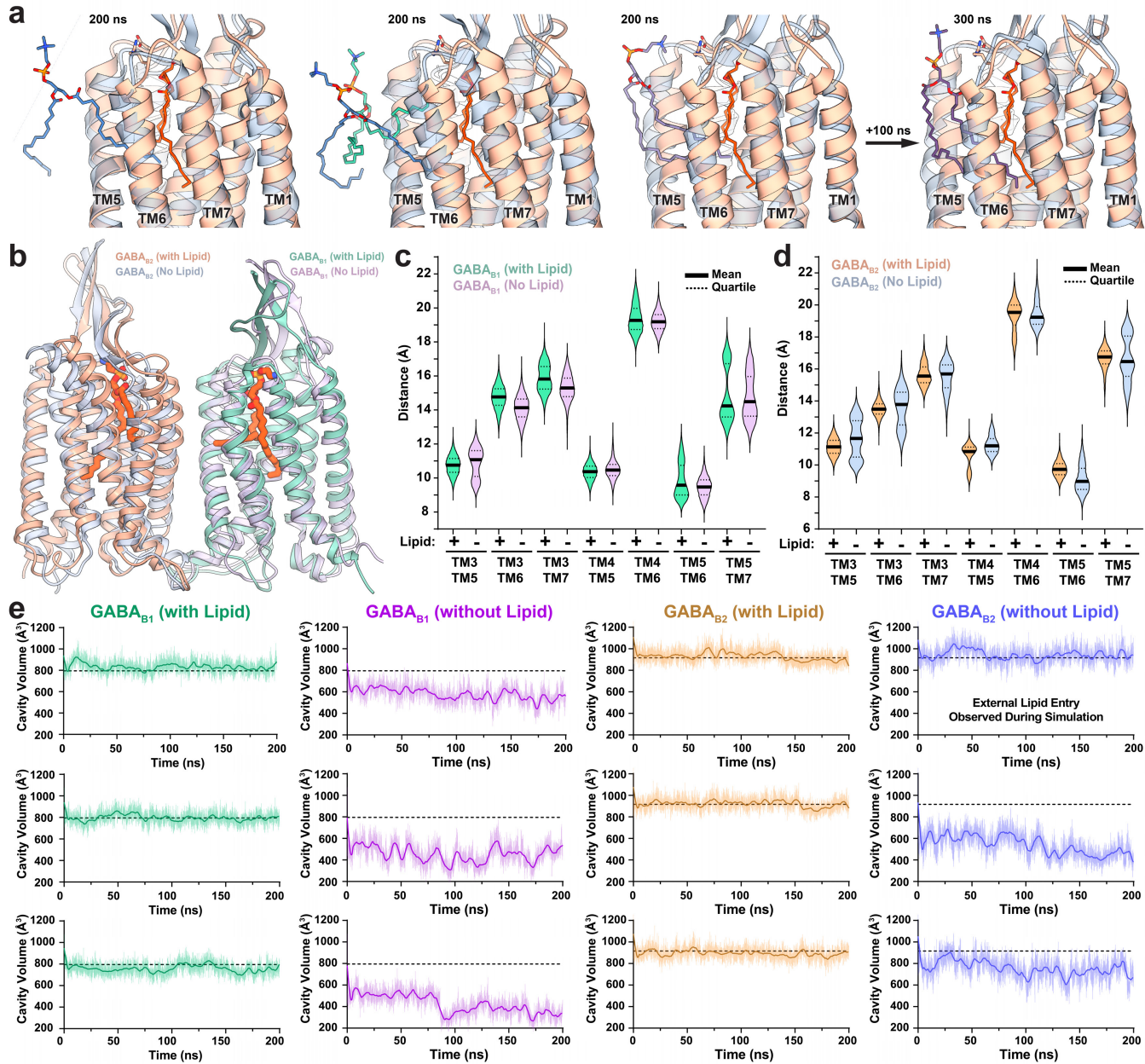
Supplemental Figure 2. Agreement between cryoEM map and model. a, EM density and model for GABA_B heterodimer complex; transmembrane helices of GABA_{B1}, transmembrane helices of GABA_{B2}, bound PE, and ligand CGP55845. Densities visualized within UCSF Chimera⁴⁵ and zoned at 2.2 with threshold set to 0.0142, with the exception of GABA_{B1}-bound lipid and GABA_{B1}-bound CGP55845 in which thresholds of 0.01 and 0.0189 were used, respectively. **b,** EM density and model for GABA_{B1} homodimer; transmembrane helices of both protomers, 7TM-bound PE, and ligand CGP55845. Densities were zoned at 2.2 and threshold set to 0.016, apart from CGP55845 in both protomers in which a threshold of 0.03 was used.



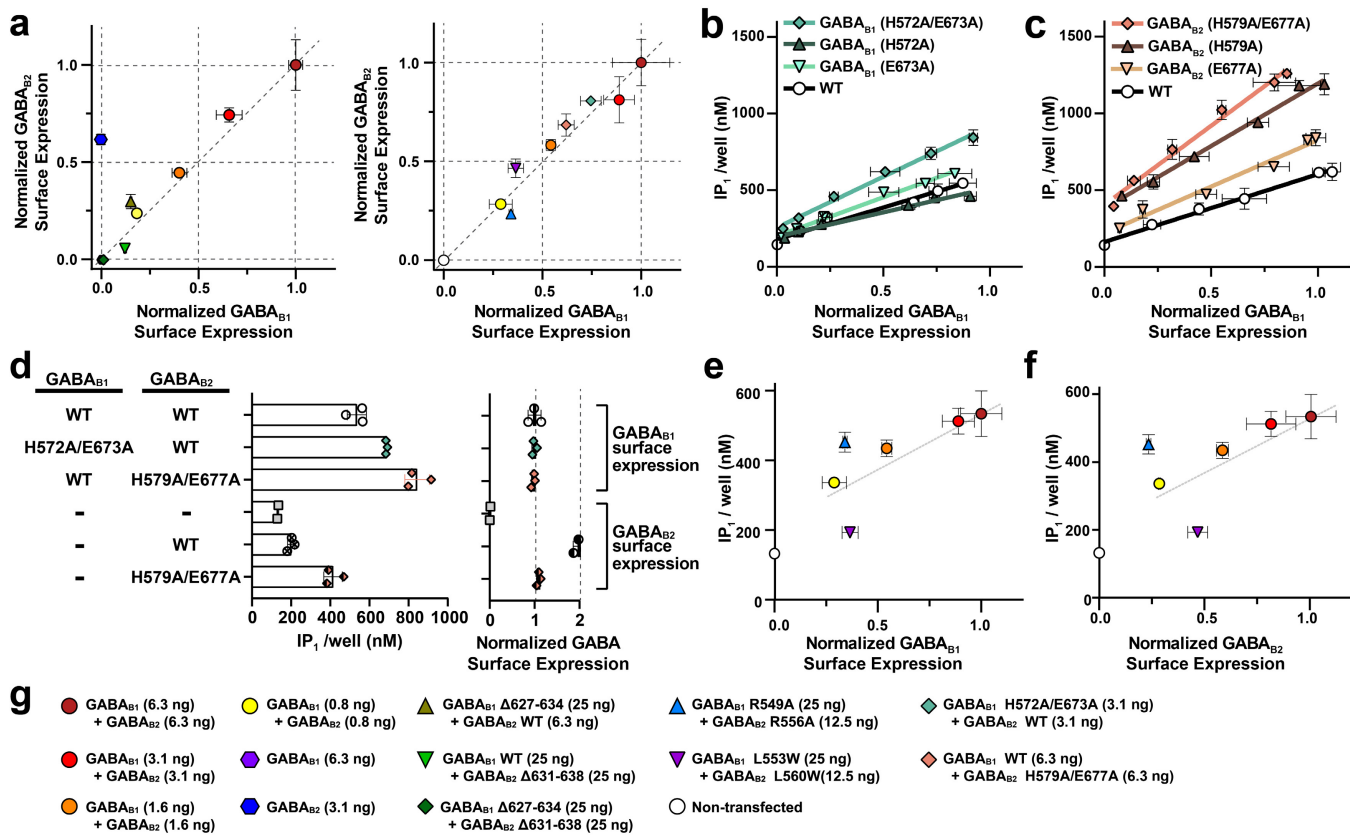
Supplemental Figure 3. Binding of CGP55845 and cation to GABA_{B1} VFT domain. **a**, Model of CGP55845 within the VFT of GABA_{B1b}. **b**, Schematic of interacting residues on GABA_{B1b} with the inhibitor, CGP55845. GABA_{B1b} residues S153 and S130 form hydrogen bonds with oxygen atoms of the phosphate group, while H170 and E349 form a hydrogen bond and a salt bridge with the amine group of the ligand, respectively. π - π stacking occurs between the chlorinated ring structure of CGP55845 and W278, while W65 provides hydrophobic packing on the opposing side of the ring. S130, H170, E349, and W65 are all substantially different residues in GABA_{B2}, precluding ligand binding. Residues are color-coded corresponding to their properties: light blue, hydrophilic; orange, anionic; green, hydrophobic; yellow, glycine; and grey, cysteine. Interaction lines are also color-coded according to their type: light blue, side-chain hydrogen bonding; grey, backbone hydrogen bonding; blue-red gradient, salt-bridge; and green, π - π stacking. **c**, Spherical density surrounded by anionic residues within the VFT supports a cation (magenta) at that site.



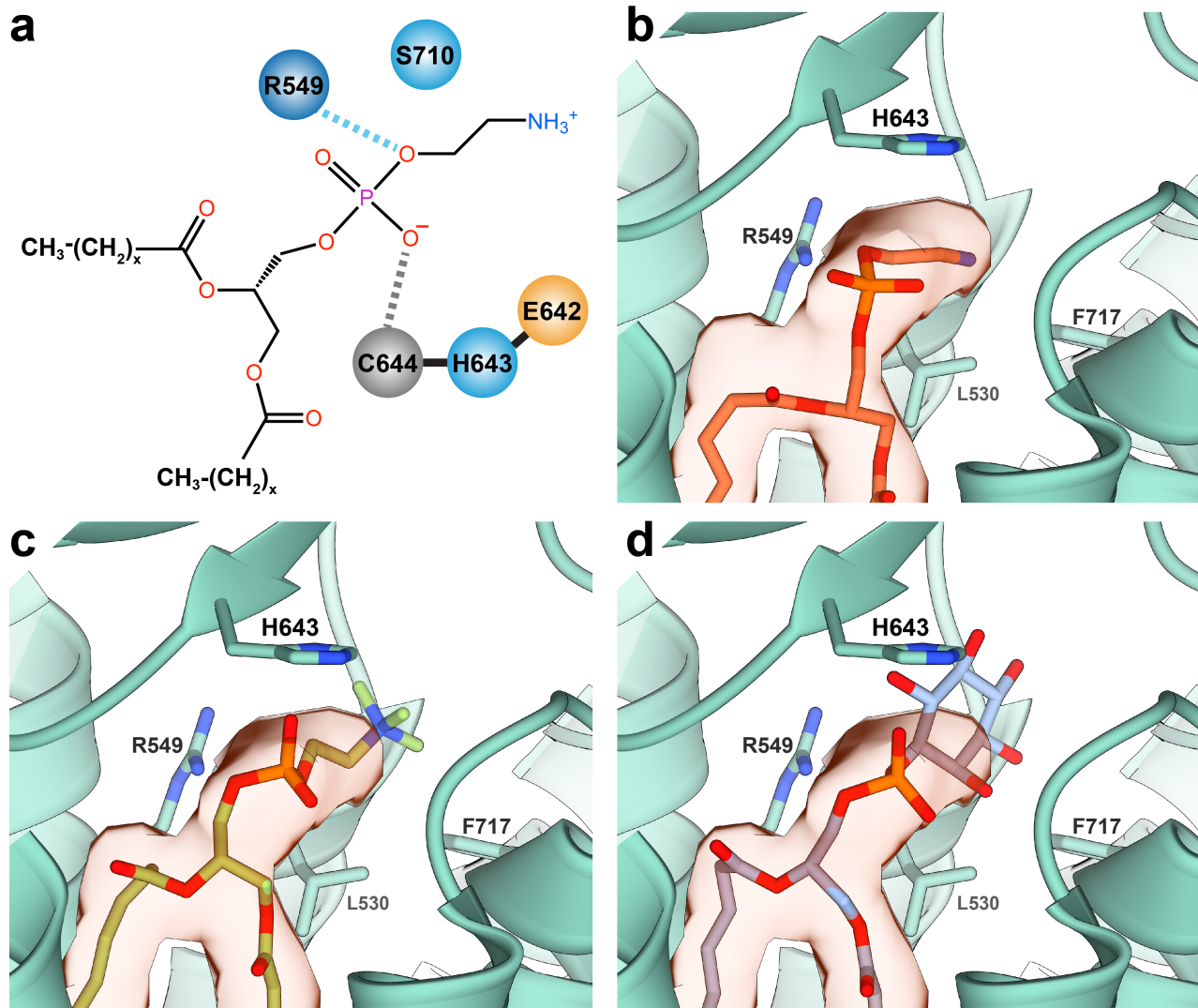
Supplemental Figure 4. Comparison of structures across GPCR classes. **a**, GABA_B protomers share similar secondary and overall structure. **b**, Comparison of mGlu5 and GABA_B 7TM and ECL2/linker shown from side view. **c**, Top-down view of GABA_{B1}, GABA_{B2}, mGlu5 (PDB: 6N52), and class A M2 acetylcholine receptor (PDB: 3UON) with side-chains corresponding to the “toggle-switch” motif shown. Phospholipid space-filling model is included in gray within GABA_{B1} and GABA_{B2}. **d**, Sequence alignment of human GABA_B receptors with mGlu5 and M2 receptors comparing canonical GPCR activation motifs: TM3-TM6 ionic lock (blue), “toggle switch motif” (green), FxPKxY motif (yellow). Sequences are aligned to motifs within each TM helix and transmembrane helical secondary structure is underlined. Residues in GABA_B sequences differing from canonical motifs are outlined in pink. The cysteine residue that replaces the “toggle-switch” tryptophan is highlighted in pink.



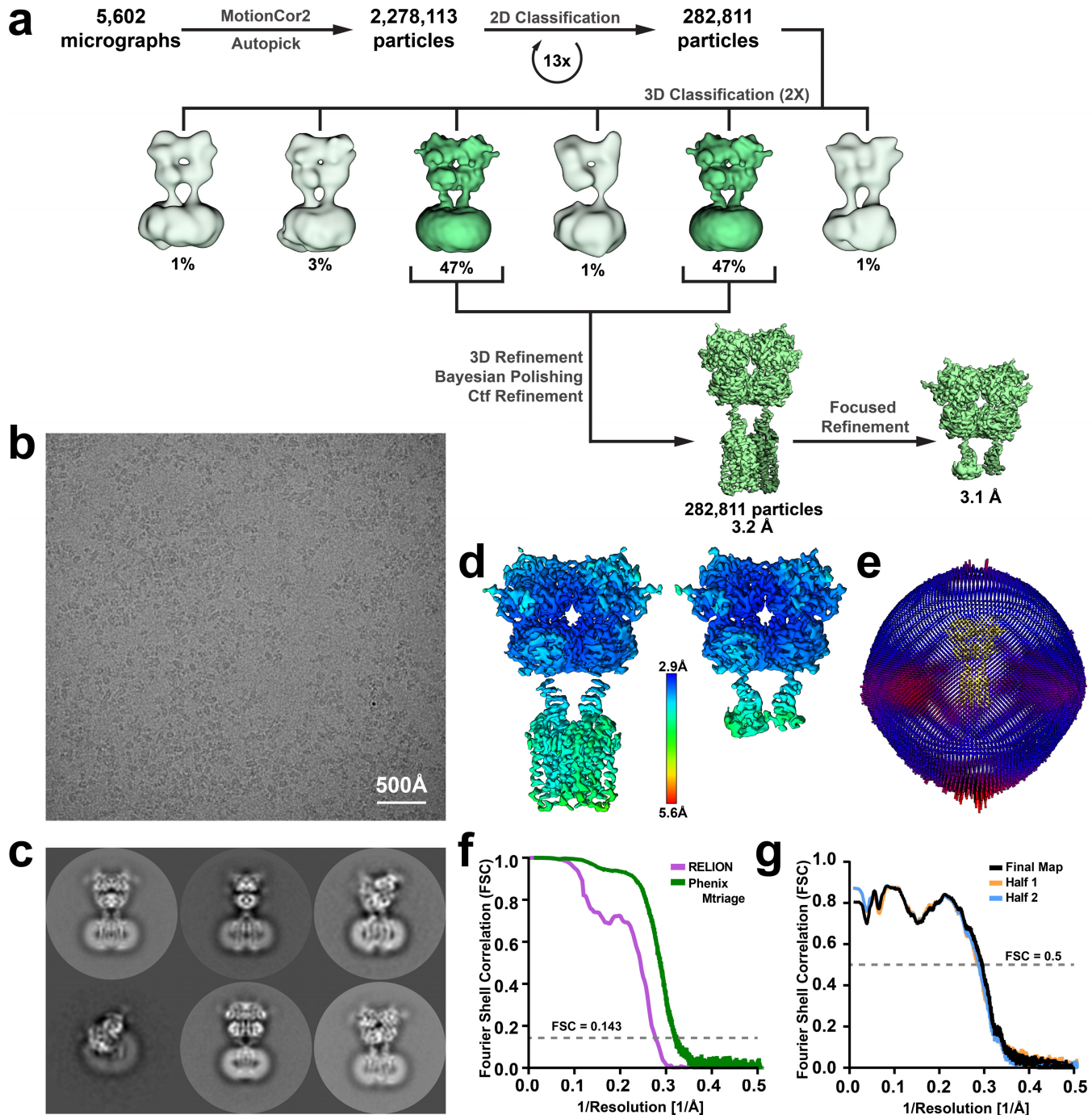
Supplemental Figure 5. Atomistic simulations of phospholipid structural stabilization and entry. **a**, The results of three out of seven total simulations of GABA_B 7TM and linker in the absence of core-bound lipid after 200 ns. The results show the extent of lipid (green, purple) entry in GABA_{B2} (grey) in the simulations versus the experimental structure (tan) with PE (orange). One of the trajectories was extended an additional 100 ns (rightmost panel) and lipid entry was observed to progress towards the core. **b**, Representative side view of the GABA_B ribbon and stick model from simulations at 200 ns showing rigidity of ECL2 β -sheet structure even in absence of VFT domains. **c**, **d**, Violin plots of ensemble distances between GABA_{B1} (**d**) and GABA_{B2} (**e**) TM helices in simulations with and without core-bound lipid. Distances were measured from the C α atoms of the following residues in GABA_{B1}: L550 (TM3), W611 (TM4), L653 (TM5), M707 (TM6), A716 (TM7); and the following residues in GABA_{B2}: T557 (TM3), W615 (TM4), L657 (TM5), F711 (TM6), Q720 (TM7). Simulations were run in triplicate over 200ns and violin plots represent 25,000 data points per condition. **e**, 7TM cavity volume measured over time for individual simulations. Average cavity volume of phospholipid-bound receptor is shown as dashed line, thick lines indicate rolling averages of 5.33 ns, and thin lines represent raw data.



Supplemental Figure 6. Functional analysis of GABA_B mutants. **a**, Comparative normalized surface expression levels of constructs assessed by FLAG-tagged GABA_{B1} and HA-tagged GABA_{B2} surface expression. **b, c**, Mutations of ionic residues forming the interface of GABA_{B1} (**b**) and GABA_{B2} (**c**) result in increased constitutive activity of the receptor. **d**, GABA_{B2} H579A/E677A expressed without GABA_{B1} shows a moderate increase in basal activity over wild-type GABA_{B2} expressed alone. **e, f**, Mutation of lipid coordinating residues (blue triangle) increase the constitutive activity of GABA_{B1} (**e**) and GABA_{B2} (**f**), while mutations displacing the lipid tails from the 7TM core (purple triangle) result in decreased basal activity of the receptor when compared to wild-type receptor of similar receptor surface expression. **g**, Key to colors and symbols used in panels **a**, **e**, and **f** with DNA transfection amounts indicated in parenthesis. Data are representative of one experiment performed in triplicate and repeated independently at least three times with similar results.



Supplemental Figure 7. Modeling of phospholipid into GABA_{B1}. **a**, Schematic of GABA_{B1} residues interacting with the polar head group of phosphatidylethanolamine (PE). The terminal amine (-NH³⁺) forms a salt bridge with residue D714^{ECL3}, while the phosphate group is coordinated by S710^{ECL3}, R549^{TM3}, and the backbone nitrogen of C644^{ECL2}. **b-d**, As our receptor purification did not contribute additional lipid, we considered the known lipid composition of Sf9 insect cells. Four primary phospholipids are present in Sf9 insect cells: phosphatidylcholine (43%), phosphatidylethanolamine (32%), phosphatidylinositol (23%), and cardiolipin (4%)⁶¹. It was apparent from the map that the lipid had only two carbon chains, immediately excluding cardiolipin as it has four hydrocarbon tails. A comparison of the map and the binding site residues led to the decision to model PE **(b)** into the pocket using the GemSpot pipeline²¹, which produced good cross-correlation with favorable interactions. To further confirm our selection, analysis of overlays of phosphatidylcholine **(c)** and phosphatidylinositol **(d)** over the docked model revealed phosphatidylcholine is unlikely given that the interactions with the cation appear to be primarily salt bridges, rather than the cation-π interactions that more commonly coordinate choline in proteins⁶². Although phosphatidylinositol may make favorable interactions, our map does not appear to support such a large moiety in the head group position. Thus, PE is the most likely lipid to reside in the structure and was thus used in the models.



Supplemental Figure 8. CryoEM processing workflow of GABA_{B1b} homodimer. **a**, Flow chart outlining the cryoEM processing of the GABA_B homodimer. **b, c**, Representative micrograph (**b**) and 2D class averages (**c**). **d**, Local resolution of cryoEM maps. **e**, Angular distribution of projections employed in the final cryoEM reconstruction. **f, g**, Gold standard FSC curve of half-maps calculated using RELION and Phenix Mtriage⁶⁰ (**f**), and map-to-model validation curves generated through Phenix Mtriage (**g**). Global indicated resolutions of the full-length structure and VFT structure were 3.2 Å and 3.1 Å, respectively, at 0.143 Fourier shell correlation (FSC) as calculated by RELION.

Supplemental Table 1. Cryo-EM data collection, refinement and validation statistics

| | GABA_{B1b}/GABA_{B2} Heterodimer | | GABA_{B1b} Homodimer |
|---|---|--------------------|-------------------------------------|
| Data collection and processing | Data Set #1 | Data Set #2 | |
| Magnification (x) | 57,050 | 57,050 | 47,198 |
| Voltage (kV) | 300 | 300 | 300 |
| Electron exposure (e ⁻ /Å ²) | 56.5 | 64.2 | 49.7 |
| Defocus range (μm) | -1.5 - -2.7 | -1.2 - -2.5 | -0.9 - -2.5 |
| Pixel size (Å) | 0.8521 | 0.8521 | 1.06 |
| Symmetry imposed | C1 | C1 | C1 |
| Initial particle images (no.) | 538,957 | 2,062,083 | 2,278,113 |
| Final particle images (no.) | 286,140 (Combined Data Sets) | | 282,811 |
| Map resolution (Å) | 3.6 Å | | 3.2 Å |
| FSC threshold | 0.143 | | 0.143 |
| Map resolution range (Å) | 3.3 - 4.4 | | 3.0 - 4.4 |
| Map sharpening B factor (Å ²) | -183.273 | | -84.088 |
| Refinement | | | |
| Initial model used (PDB code) | 4MR7, 6N52 Homology | | GABA _{B1b} of Heterodimer |
| Model resolution (Å) | 3.7 | | 3.4 |
| FSC threshold | 0.5 | | 0.5 |
| Model composition | | | |
| Non-hydrogen atoms | 9860 | | 9721 |
| Protein residues | 1345 | | 1327 |
| Ligands | 3 | | 4 |
| B factors (Å²) | | | |
| Protein | 15.17 | | 57.57 |
| Ligand | 28.97 | | 59.82 |
| R.m.s. deviations | | | |
| Bond lengths (Å) | 0.004 | | 0.007 |
| Bond angles (°) | 0.608 | | 0.763 |
| Validation | | | |
| MolProbity score | 1.75 | | 2.02 |
| Clashscore | 5.55 | | 9.98 |
| Poor rotamers (%) | 0.00 | | 0.12 |
| Ramachandran plot | | | |
| Favored (%) | 92.92 | | 91.66 |
| Allowed (%) | 7.08 | | 8.34 |
| Disallowed (%) | 0.00 | | 0.00 |

Supplemental Table 2. Basal, Emax and GABA potency estimates of GABA-B ECL2 deletion mutants in HEK293 cells co-transfected with Gqo5

| GABA-B receptor | sub | IP1 accumulation at 20 mM LiCl | | | | GABA-induced IP1 accumulation at 20 mM LiCl | | | | | | | | | | n |
|--|-----|--------------------------------|------------|--------------|------------|---|--------------|-----------|-------------|------------|--------------|------------------|------------|--------------|--|---|
| | | Basal activity ± SEM | comparison | P-value | Emax ± SEM | comparison | P-value | EC50 (μM) | pEC50 ± SEM | comparison | P-value | Hill slope ± SEM | comparison | P-value | | |
| GB1-wt + GB2-wt (6.3+6.3 ng) | 1 | 2.3 ± 0.14 | | | 9.3 ± 0.40 | | | 0.31 | 6.50 ± 0.06 | | | 0.70 ± 0.06 | | | | 7 |
| GB1-wt + GB2-wt (3.1+3.1 ng) | 2 | 2.1 ± 0.09 | 1 vs 2 | >0.9616 (ns) | 7.6 ± 0.46 | 1 vs 2 | 0.0089 | 0.32 | 6.49 ± 0.03 | 1 vs 2 | >0.9999 (ns) | 0.66 ± 0.04 | 1 vs 2 | >0.9999 (ns) | | 7 |
| GB1-wt + GB2-wt (1.6+1.6 ng) | 3 | 1.7 ± 0.07 | 1 vs 3 | 0.0426 | 6.2 ± 0.32 | 1 vs 3 | <0.0001 | 0.34 | 6.47 ± 0.12 | 1 vs 3 | >0.9999 (ns) | 0.68 ± 0.06 | 1 vs 3 | >0.9999 (ns) | | 7 |
| GB1-wt + GB2-wt (0.8+0.8 ng) | 4 | 1.6 ± 0.12 | 1 vs 4 | 0.0072 | 4.7 ± 0.30 | 1 vs 4 | <0.0001 | 0.38 | 6.42 ± 0.11 | 1 vs 4 | 0.9974 (ns) | 0.82 ± 0.05 | 1 vs 4 | 0.9435 (ns) | | 6 |
| GB1-wt only (6.3 ng) | 5 | 1.2 ± 0.17 | no stats | n.d | 1.1 ± 0.11 | no stats | n.d | n.d" | n.d" | no stats | n.d | n.d" | no stats | n.d | | 6 |
| GB2-wt only (3.1 ng) | 6 | 1.3 ± 0.11 | no stats | n.d | 1.2 ± 0.12 | no stats | n.d | n.d" | n.d" | no stats | n.d | n.d" | no stats | n.d | | 6 |
| non-transfected | 7 | 1.1 ± 0.04 | no stats | n.d | 1.0 ± 0.04 | no stats | n.d | n.d" | n.d" | no stats | n.d | n.d" | no stats | n.d | | 6 |
| GB1-Δ627-634 + GB2-wt (25+6.3 ng) | 8 | 4.3 ± 0.32 | 4 vs 8 | <0.0001 | 8.1 ± 0.58 | 4 vs 8 | <0.0001 | 1.04 | 5.98 ± 0.03 | 4 vs 8 | 0.0046 | 0.97 ± 0.07 | 4 vs 8 | 0.7753 (ns) | | 7 |
| GB1-wt + GB2-Δ631-638 (25+25 ng) | 9 | 1.5 ± 0.10 | 4 vs 9 | >0.9999 (ns) | 7.4 ± 0.48 | 4 vs 9 | <0.0001 | 1.49 | 5.83 ± 0.06 | 4 vs 9 | <0.0001 | 0.87 ± 0.08 | 4 vs 9 | 0.9995 (ns) | | 7 |
| GB1-Δ627-634 + GB2-Δ631-638 (25+25 ng) | 10 | 1.1 ± 0.09 | 4 vs 10 | 0.3389 (ns) | 1.8 ± 0.13 | 4 vs 10 | <0.0001 | 6.43 | 5.19 ± 0.08 | 4 vs 10 | <0.0001 | 1.14 ± 0.16 | 4 vs 10 | 0.054 (ns) | | 5 |
| GB1-L553W + GB2-L560W (25+13 ng) | 11 | 1.3 ± 0.14 | 3 vs 11 | 0.6510 (ns) | 8.8 ± 0.42 | 3 vs 11 | 0.0001 | 0.93 | 6.03 ± 0.14 | 3 vs 11 | 0.0072 | 0.92 ± 0.05 | 3 vs 11 | 0.2819 (ns) | | 5 |
| GB1-R549A + GB2-R556A (25+13 ng) | 12 | 2.1 ± 0.18 | 3 vs 12 | 0.6325 (ns) | 8.3 ± 0.49 | 3 vs 12 | 0.0056 | 0.12 | 6.93 ± 0.10 | 3 vs 12 | 0.0106 | 0.82 ± 0.03 | 3 vs 12 | 0.9201 (ns) | | 4 |
| GB1-H572A/E673A + GB2-wt (3.1+3.1 ng) | 13 | 2.7 ± 0.42 | 2 vs 13 | 0.3035 (ns) | 7.6 ± 0.62 | 2 vs 13 | >0.9999 (ns) | 0.17 | 6.78 ± 0.14 | 2 vs 13 | 0.3766 (ns) | 0.56 ± 0.16 | 2 vs 13 | 0.9955 (ns) | | 3 |
| GB1-wt + GB2-H579A/E677A (6.3+6.3 ng) | 14 | 3.9 ± 0.23 | 2 vs 14 | <0.0001 | 7.4 ± 0.48 | 2 vs 14 | >0.9999 (ns) | n.d" | n.d" | no stats | n.d | n.d" | no stats | n.d | | 3 |

Statistics were performed by one-way ANOVA, followed by Sidak's multiple comparisons test as indicated

For comparison of mutant with wild type values, the wild type value selected for comparison was the condition with similar surface expression level as the mutant (see Extended figure 6)

Each p-value was adjusted to account for multiple comparisons

n.d., not determined; n.d", not determined as no GABA-induced response or fitted curve

References

- 1 Bowery, N. G. & Smart, T. G. GABA and glycine as neurotransmitters: a brief history. *Br J Pharmacol* **147 Suppl 1**, S109-119, doi:10.1038/sj.bjp.0706443 (2006).
- 2 Mannoury la Cour, C., Herbelles, C., Pasteau, V., de Nanteuil, G. & Millan, M. J. Influence of positive allosteric modulators on GABA(B) receptor coupling in rat brain: a scintillation proximity assay characterisation of G protein subtypes. *J Neurochem* **105**, 308-323, doi:10.1111/j.1471-4159.2007.05131.x (2008).
- 3 Franek, M. *et al.* The heteromeric GABA-B receptor recognizes G-protein alpha subunit C-termini. *Neuropharmacology* **38**, 1657-1666, doi:10.1016/s0028-3908(99)00135-5 (1999).
- 4 Hepler, J. R. & Gilman, A. G. G proteins. *Trends Biochem Sci* **17**, 383-387 (1992).
- 5 Fatemi, S. H., Folsom, T. D. & Thuras, P. D. Deficits in GABA(B) receptor system in schizophrenia and mood disorders: a postmortem study. *Schizophr Res* **128**, 37-43, doi:10.1016/j.schres.2010.12.025 (2011).
- 6 Enna, S. J. GABAB receptor agonists and antagonists: pharmacological properties and therapeutic possibilities. *Expert Opin Investig Drugs* **6**, 1319-1325, doi:10.1517/13543784.6.10.1319 (1997).
- 7 Malcangio, M. GABAB receptors and pain. *Neuropharmacology* **136**, 102-105, doi:10.1016/j.neuropharm.2017.05.012 (2018).
- 8 Froestl, W. in *Advances in Pharmacology* Vol. 58 (ed Thomas P. Blackburn) 19-62 (Academic Press, 2010).
- 9 Albright, A. L. Baclofen in the treatment of cerebral palsy. *J Child Neurol* **11**, 77-83, doi:10.1177/088307389601100202 (1996).
- 10 Pin, J. P., Galvez, T. & Prezeau, L. Evolution, structure, and activation mechanism of family 3/C G-protein-coupled receptors. *Pharmacology & therapeutics* **98**, 325-354, doi:10.1016/s0163-7258(03)00038-x (2003).
- 11 Brauner-Osborne, H., Wellendorph, P. & Jensen, A. A. Structure, pharmacology and therapeutic prospects of family C G-protein coupled receptors. *Curr Drug Targets* **8**, 169-184, doi:10.2174/138945007779315614 (2007).
- 12 Chun, L., Zhang, W. H. & Liu, J. F. Structure and ligand recognition of class C GPCRs. *Acta Pharmacol Sin* **33**, 312-323, doi:10.1038/aps.2011.186 (2012).

13 Geng, Y., Bush, M., Mosyak, L., Wang, F. & Fan, Q. R. Structural mechanism of ligand activation in human GABA(B) receptor. *Nature* **504**, 254-259, doi:10.1038/nature12725 (2013).

14 Geng, Y. *et al.* Structural mechanism of ligand activation in human calcium-sensing receptor. *eLife* **5**, doi:10.7554/eLife.13662 (2016).

15 Koehl, A. *et al.* Structural insights into the activation of metabotropic glutamate receptors. *Nature* **566**, 79-84, doi:10.1038/s41586-019-0881-4 (2019).

16 Margeta-Mitrovic, M., Jan, Y. N. & Jan, L. Y. A Trafficking Checkpoint Controls GABAB Receptor Heterodimerization. *Neuron* **27**, 97-106, doi:10.1016/S0896-6273(00)00012-X (2000).

17 Robbins, M. J. *et al.* GABAB2 Is Essential for G-Protein Coupling of the GABAB Receptor Heterodimer. *The Journal of Neuroscience* **21**, 8043-8052, doi:10.1523/jneurosci.21-20-08043.2001 (2001).

18 Galvez, T. *et al.* Mutagenesis and modeling of the GABAB receptor extracellular domain support a venus flytrap mechanism for ligand binding. *J Biol Chem* **274**, 13362-13369, doi:10.1074/jbc.274.19.13362 (1999).

19 Hannan, S., Wilkins, M. E. & Smart, T. G. Sushi domains confer distinct trafficking profiles on GABAB receptors. *Proceedings of the National Academy of Sciences of the United States of America* **109**, 12171-12176, doi:10.1073/pnas.1201660109 (2012).

20 Mukherjee, R. S., McBride, E. W., Beinborn, M., Dunlap, K. & Kopin, A. S. Point mutations in either subunit of the GABAB receptor confer constitutive activity to the heterodimer. *Molecular pharmacology* **70**, 1406-1413, doi:10.1124/mol.106.024463 (2006).

21 Robertson, M. J., van Zundert, G. C. P., Borrelli, K. & Skiniotis, G. GemSpot: A Pipeline for Robust Modeling of Ligands into CryoEM Maps. *bioRxiv*, 750778, doi:10.1101/750778 (2019).

22 Kato, K., Goto, M. & Fukuda, H. Regulation by divalent cations of 3H-baclofen binding to GABAB sites in rat cerebellar membranes. *Life sciences* **32**, 879-887, doi:10.1016/0024-3205(83)90225-4 (1983).

23 Bowery, N. G., Hill, D. R. & Hudson, A. L. Characteristics of GABAB receptor binding sites on rat whole brain synaptic membranes. 1983. *British journal of pharmacology* **100**, 452-467; discussion 450-451, doi:10.1111/j.1476-5381.1997.tb06835.x (1997).

24 Conklin, B. R., Farfel, Z., Lustig, K. D., Julius, D. & Bourne, H. R. Substitution of three amino acids switches receptor specificity of Gq alpha to that of Gi alpha. *Nature* **363**, 274-276, doi:10.1038/363274a0 (1993).

25 Trinquet, E. *et al.* D-myo-inositol 1-phosphate as a surrogate of D-myo-inositol 1,4,5-tris phosphate to monitor G protein-coupled receptor activation. *Analytical biochemistry* **358**, 126-135, doi:10.1016/j.ab.2006.08.002 (2006).

26 Liu, J. *et al.* Molecular determinants involved in the allosteric control of agonist affinity in the GABAB receptor by the GABAB2 subunit. *J Biol Chem* **279**, 15824-15830, doi:10.1074/jbc.M313639200 (2004).

27 Audet, M. & Stevens, R. C. Emerging structural biology of lipid G protein-coupled receptors. *Protein science : a publication of the Protein Society* **28**, 292-304, doi:10.1002/pro.3509 (2019).

28 Doré, A. S. *et al.* Structure of class C GPCR metabotropic glutamate receptor 5 transmembrane domain. *Nature* **511**, 557-562, doi:10.1038/nature13396 (2014).

29 Frangaj, A. & Fan, Q. R. Structural biology of GABAB receptor. *Neuropharmacology* **136**, 68-79, doi:10.1016/j.neuropharm.2017.10.011 (2018).

30 Gasparini, F. & Spooren, W. Allosteric modulators for mGlu receptors. *Curr Neuropharmacol* **5**, 187-194, doi:10.2174/157015907781695900 (2007).

31 Hyland, N. P. & Cryan, J. F. A Gut Feeling about GABA: Focus on GABA(B) Receptors. *Front Pharmacol* **1**, 124, doi:10.3389/fphar.2010.00124 (2010).

32 Ng, T. K. & Yung, K. K. Differential expression of GABA(B)R1 and GABA(B)R2 receptor immunoreactivity in neurochemically identified neurons of the rat neostriatum. *The Journal of comparative neurology* **433**, 458-470, doi:10.1002/cne.1153 (2001).

33 Burman, K. J. *et al.* GABAB receptor subunits, R1 and R2, in brainstem catecholamine and serotonin neurons. *Brain Res* **970**, 35-46, doi:10.1016/s0006-8993(02)04269-5 (2003).

34 Calver, A. R. *et al.* The expression of GABA(B1) and GABA(B2) receptor subunits in the CNS differs from that in peripheral tissues. *Neuroscience* **100**, 155-170, doi:10.1016/s0306-4522(00)00262-1 (2000).

35 Gassmann, M. *et al.* Redistribution of GABAB(1) protein and atypical GABAB responses in GABAB(2)-deficient mice. *The Journal of neuroscience : the official journal of the Society for Neuroscience* **24**, 6086-6097, doi:10.1523/JNEUROSCI.5635-03.2004 (2004).

36 Margeta-Mitrovic, M., Jan, Y. N. & Jan, L. Y. Ligand-induced signal transduction within heterodimeric GABA(B) receptor. *Proc Natl Acad Sci U S A* **98**, 14643-14648, doi:10.1073/pnas.251554798 (2001).

37 Xue, L. *et al.* Rearrangement of the transmembrane domain interfaces associated with the activation of a GPCR hetero-oligomer. *Nat Commun* **10**, 2765, doi:10.1038/s41467-019-10834-5 (2019).

38 Binet, V. *et al.* The heptahelical domain of GABA(B2) is activated directly by CGP7930, a positive allosteric modulator of the GABA(B) receptor. *The Journal of biological chemistry* **279**, 29085-29091, doi:10.1074/jbc.M400930200 (2004).

39 Guan, X. M., Kobilka, T. S. & Kobilka, B. K. Enhancement of membrane insertion and function in a type IIIb membrane protein following introduction of a cleavable signal peptide. *The Journal of biological chemistry* **267**, 21995-21998 (1992).

40 Mastronarde, D. N. Automated electron microscope tomography using robust prediction of specimen movements. *Journal of structural biology* **152**, 36-51, doi:10.1016/j.jsb.2005.07.007 (2005).

41 Zheng, S. Q. *et al.* MotionCor2: anisotropic correction of beam-induced motion for improved cryo-electron microscopy. *Nature methods* **14**, 331-332, doi:10.1038/nmeth.4193 (2017).

42 Zhang, K. Gctf: Real-time CTF determination and correction. *Journal of structural biology* **193**, 1-12, doi:10.1016/j.jsb.2015.11.003 (2016).

43 Rohou, A. & Grigorieff, N. CTFFIND4: Fast and accurate defocus estimation from electron micrographs. *Journal of structural biology* **192**, 216-221, doi:10.1016/j.jsb.2015.08.008 (2015).

44 Zivanov, J. *et al.* New tools for automated high-resolution cryo-EM structure determination in RELION-3. *eLife* **7**, doi:10.7554/eLife.42166 (2018).

45 Pettersen, E. F. *et al.* UCSF Chimera--a visualization system for exploratory research and analysis. *J Comput Chem* **25**, 1605-1612, doi:10.1002/jcc.20084 (2004).

46 Emsley, P., Lohkamp, B., Scott, W. G. & Cowtan, K. Features and development of Coot. *Acta crystallographica. Section D, Biological crystallography* **66**, 486-501, doi:10.1107/s0907444910007493 (2010).

47 Liebschner, D. *et al.* Macromolecular structure determination using X-rays, neutrons and electrons: recent developments in Phenix. *Acta crystallographica. Section D, Structural biology* **75**, 861-877, doi:10.1107/s2059798319011471 (2019).

48 Lomize, M. A., Pogozheva, I. D., Joo, H., Mosberg, H. I. & Lomize, A. L. OPM database and PPM web server: resources for positioning of proteins in membranes. *Nucleic acids research* **40**, D370-376, doi:10.1093/nar/gkr703 (2012).

49 Jo, S., Kim, T., Iyer, V. G. & Im, W. CHARMM-GUI: a web-based graphical user interface for CHARMM. *J Comput Chem* **29**, 1859-1865, doi:10.1002/jcc.20945 (2008).

50 Humphrey, W., Dalke, A. & Schulten, K. VMD: visual molecular dynamics. *J Mol Graph* **14**, 33-38, 27-38, doi:10.1016/0263-7855(96)00018-5 (1996).

51 Phillips, J. C. *et al.* Scalable molecular dynamics with NAMD. *J Comput Chem* **26**, 1781-1802, doi:10.1002/jcc.20289 (2005).

52 Robertson, M. J., Tirado-Rives, J. & Jorgensen, W. L. Improved Peptide and Protein Torsional Energetics with the OPLSAA Force Field. *J Chem Theory Comput* **11**, 3499-3509, doi:10.1021/acs.jctc.5b00356 (2015).

53 Ryckaert, J.-P., Ciccotti, G. & Berendsen, H. J. C. Numerical integration of the cartesian equations of motion of a system with constraints: molecular dynamics of n-alkanes. *Journal of Computational Physics* **23**, 327-341, doi:10.1016/0021-9991(77)90098-5 (1977).

54 Miyamoto, S. & Kollman, P. A. Settle - an Analytical Version of the Shake and Rattle Algorithm for Rigid Water Models. *Journal of Computational Chemistry* **13**, 952-962, doi:DOI 10.1002/jcc.540130805 (1992).

55 Laurent, B. *et al.* Epoch: rapid analysis of protein pocket dynamics. *Bioinformatics (Oxford, England)* **31**, 1478-1480, doi:10.1093/bioinformatics/btu822 (2015).

56 Ballesteros, J. A. & Weinstein, H. in *Methods in Neurosciences* Vol. 25 (ed Stuart C. Sealfon) 366-428 (Academic Press, 1995).

57 Hilger, D. *et al.* Structural insights into ligand efficacy and activation of the glucagon receptor. *bioRxiv*, 660837, doi:10.1101/660837 (2019).

58 Towns, J. *et al.* XSEDE: Accelerating Scientific Discovery. *Computing in Science & Engineering* **16**, 62-74, doi:Doi 10.1109/Mcse.2014.80 (2014).

59 Scheres, S. H. Processing of Structurally Heterogeneous Cryo-EM Data in RELION. *Methods in enzymology* **579**, 125-157, doi:10.1016/bs.mie.2016.04.012 (2016).

60 Afonine, P. V. *et al.* New tools for the analysis and validation of cryo-EM maps and atomic models. *Acta crystallographica. Section D, Structural biology* **74**, 814-840, doi:10.1107/S2059798318009324 (2018).

61 Marheineke, K., Grunewald, S., Christie, W. & Reilander, H. Lipid composition of *Spodoptera frugiperda* (Sf9) and *Trichoplusia ni* (Tn) insect cells used for baculovirus infection. *FEBS Lett* **441**, 49-52, doi:10.1016/s0014-5793(98)01523-3 (1998).

62 Ma, J. C. & Dougherty, D. A. The Cationminus signpi Interaction. *Chemical reviews* **97**, 1303-1324, doi:10.1021/cr9603744 (1997).